Article

Quantum memories : a review based on the European integrated project "Qubit Applications (QAP)"

SIMON, Christoph, *et al*.

Abstract

We perform a review of various approaches to the implementation of quantum memories, with an emphasis on activities within the quantum memory sub-project of the EU integrated project "Qubit Applications". We begin with a brief overview over different applications for quantum memories and different types of quantum memories. We discuss the most important criteria for assessing quantum memory performance and the most important physical requirements. Then we review the different approaches represented in "Qubit Applications" in some detail. They include solid-state atomic ensembles, NV centers, quantum dots, single atoms, atomic gases and optical phonons in diamond. We compare the different approaches using the discussed criteria.

Reference

UNIVERSITÉ
DE GENÈVE

Quantum Memories

A Review based on the European Integrated Project "Qubit Applications (QAP)"

Christoph Simon[1,9], Mikael Afzelius[1], Jürgen Appel[2], Antoine Boyer de la Giroday[6], Samuel J. Dewhurst[6] Nicolas Gisin[1], Chengyong Hu[7], Fedor Jelezko[3], Stefan Kröll[4], Jörg Helge Müller[2], Joshua Nunn[5], Eugene Polzik[2], John Rarity[7], Hugues de Riedmatten[1], Wenjamin Rosenfeld[8], Andrew J. Shields[6], Niklas Sköld[6], R. Mark Stevenson[6], Robert Thew[1], Ian Walmsley[5], Markus Weber[8], Harald Weinfurter[8], Jörg Wrachtrup[3], and Robert J. Young[6]

[1] Group of Applied Physics, University of Geneva, CH-1211 Geneva, Switzerland
[2] Niels Bohr Institute, Copenhagen University, Blegdamsvej 17, 2100 København Ø, Denmark
[3] 3. Physikalisches Institut, Universität Stuttgart, Stuttgart, Germany
[4] Department of Physics, Lund University, Box 118, SE-221 00 Lund, Sweden
[5] Clarendon Laboratory, University of Oxford, Oxford OX1 3PU, United Kingdom
[6] Toshiba Research Europe Limited, 208 Cambridge Science Park, Cambridge CB4 0GZ, United Kingdom
[7] Electrical and Electronic Engineering, University of Bristol, Bristol BS8 1UB, United Kingdom
[8] Ludwig-Maximilians-Universität München, D-80799 München, Germany and Max-Planck-Institut für Quantenoptik, D-85748 Garching, Germany
[9] Institute for Quantum Information Science and Department of Physics and Astronomy, University of Calgary, Calgary T2N 1N4, Canada

Abstract. We perform a review of various approaches to the implementation of quantum memories, with an emphasis on activities within the quantum memory sub-project of the EU Integrated Project "Qubit Applications". We begin with a brief overview over different applications for quantum memories and different types of quantum memories. We discuss the most important criteria for assessing quantum memory performance and the most important physical requirements. Then we review the different approaches represented in "Qubit Applications" in some detail. They include solid-state atomic ensembles, NV centers, quantum dots, single atoms, atomic gases and optical phonons in diamond. We compare the different approaches using the discussed criteria.

PACS. 03.67.-a Quantum information – 03.67.Hk Quantum communication – 03.67.Lx Quantum computation architectures and implementations – 42.50.Ct Quantum description of interaction of light and matter; related experiments – 42.50.Md Optical transient phenomena: quantum beats, photon echo, free-induction decay, dephasings and revivals, optical nutation, and self-induced transparency

1 Introduction

Quantum memories are important elements for quantum information processing applications such as quantum networks [1], quantum repeaters [2,3] and linear optics quantum computing [4,5]. The field of quantum memories has recently been very active. Recent reviews include Ref. [6], which gives a compact overview over different memory protocols with atomic ensembles, Ref. [7], which deals with ensemble-based memories with a detailed focus on atomic gases, and Ref. [8], which deals with photon-echo based quantum memories, in particular in solid-state atomic ensembles, as well as Ref. [9], which is focused on quantum memories based on electromagnetically induced transparency. Quantum memories were also discussed in the Strategic Report on quantum information processing and communication in Europe [10]. The high activity of the field was

also reflected in the European Integrated Project *Qubit Applications (QAP)*, which had a sub-project involving seven research groups devoted to the development of quantum memories. As members of this sub-project we made a sustained effort over the course of the project to compare our various approaches. This included the definition of appropriate criteria for such comparisons. The present paper has grown out of this effort. We hope that it will be useful for a wider audience.

The approaches to quantum memories represented in the project are quite diverse, including solid-state atomic ensembles in rare-earth doped crystals, NV centers in diamond, semiconductor quantum dots, single trapped atoms, room-temperature and cold atomic gases, and optical phonons in bulk diamond. It was therefore an interesting challenge to develop a common language, in order to be able to perform a meaningful comparison. We will begin this review

by discussing different applications for quantum memories in section 2, followed by a brief overview of the different meanings that the term "quantum memory" can have in section 3. We will then review the most important criteria for assessing the performance of quantum memories in section 4. Section 5 discusses two physical requirements that are important for good quantum memory performance in a range of different approaches, namely good light-matter coupling and good coherence. Section 6, which is divided in seven sub-sections, is devoted to an overview of the different physical approaches that were represented in *Qubit Applications*. In section 7 we summarize our findings. This section includes a comparative table that positions the different approaches with respect to a number of relevant criteria.

2 Applications of quantum memories

Quantum memories are important in a number of contexts, including the implementation of single-photon sources, quantum repeaters, loophole-free Bell inequality tests, communication complexity protocols and precision measurements.

2.1 Deterministic Single Photon Sources

One simple, but potentially very important application of a quantum memory is the implementation of a single-photon source. Given a non-deterministic source of photon pairs such as parametric down-conversion, one can realize a deterministic source of single photons by detecting one photon of a pair (when it is emitted), while storing the other one in a memory. Detection of the first photon signals that the memory has been "charged" and can now be used as a single-photon source. In order to implement a close to ideal single-photon source the memory has to be highly efficient. Deterministic single photon sources are important ingredients for linear optics quantum computing [4,5]. They are also useful for certain quantum repeater protocols [3,11].

2.2 Quantum Repeaters

Another area where quantum memories are absolutely essential is for the implementation of long-distance quantum communication via quantum repeaters. The direct distribution of quantum states is limited by unavoidable transmission losses in combination with the no-cloning theorem. The quantum repeater approach [2] overcomes this difficulty by combining quantum teleportation and quantum state storage. The idea is to divide a given long distance into shorter elementary links, create and store entanglement independently for each link, then extend it to the whole distance via entanglement swapping (i.e. quantum teleportation of entanglement). This approach is possible only if quantum memories are available. Requirements for quantum memories in this context include long

coherence times, efficient interfacing with photons (which serve as long-distance carriers of quantum information) and the possibility of performing entanglement swapping operations [3]. However, it is not absolutely necessary for the memories to be able to both absorb and emit photons as we assumed in our previous example for realizing a single-photon source. There are different possible approaches, cf. the next section.

2.3 Loophole-free Bell test

A more fundamental application for quantum memories is the realization of a loophole-free test of Bell's inequality. A loophole-free test requires both creating entanglement over a long distance in order to enforce the locality condition and detecting the entangled systems with high efficiency in order to close the efficiency loophole. One attractive approach towards achieving this goal is to create entanglement between distant atoms or ions via the detection of photons [12,13]. These atoms or ions can be seen as quantum memories. Their interest in the present context lies in the fact that they can be detected with high (essentially unit) efficiency. At the same time such a setup can also be seen as an elementary link of a quantum repeater.

2.4 Communication complexity and protocols requiring Local Operations and Classical Communication (LOCC)

Communication complexity, i.e. the number of qubits needed for achieving a certain communication task, has recently been shown to be tightly linked to the violation of Bell-type inequalities [14]. It may be useful to store quantum states transmitted by light in memories in order to achieve loophole free violations of this kind. Communication protocols which require LOCC use memories to perform local operations and store the results while classical communication is going on. Examples of such protocols for continuous variables include iterative continuous variable entanglement distillation [15], continuous variable cluster state quantum computation [16], communication/cryptography protocols involving several rounds [17], and quantum illumination [18].

2.5 Precision measurements

A good quantum memory is capable of storing long-lived entanglement. As such, it can be used as a resource for entanglement enhanced sensing and precision metrology applications. A standard technique to enhance the weak coupling between light and matter is to use ensembles of many atoms. This approach does not only promise efficient quantum memories [20], [21], [19], but it can also increase the precision when detecting external disturbances on the state of such a system with quantum mechanically limited resolution. By preparing a collective entangled state of the atomic ensemble (e.g. by storing a squeezed state

of light in the memory[22,23] or by squeezing a collective atomic observable via a quantum-non-demolition (QND) measurement [24]), the projection noise can be reduced. Due to the non-classical correlations between the atoms a measurement precision beyond the classical limit is possible. Already, spin squeezing on the Cesium clock transition has been demonstrated, which potentially can improve the precision of optical lattice clocks [25]. Also, an ultra-sensitive RF-magnetometer employing entanglement in a room-temperature Cs vapour cell has been successfully developed [26]. In NMR systems NOON states of 10 entangled spins have been employed to improve upon magnetic field sensing almost tenfold compared to standard measuring strategies [27].

3 Different types of quantum memories

It is useful to distinguish different ways of using quantum memories and of characterizing their performance. This includes the use of quantum memories for storing single photons, for general states of light, and memories that are charged through the emission of photons.

3.1 Memories for single photons

For applications such as the implementation of a single photon source, or quantum repeaters, one often knows that the desired output state of the memory is a single-photon state. For example, a quantum repeater protocol might involve memories that are designed to absorb and reemit photons that are emitted by other sources [11, 28] (e.g. photon-pair sources based on parametric down-conversion, or more ideal single-photon or photon-pair sources based on single atoms or quantum dots). In such a situation, it is natural to verify the performance of the memory using photon counting. The memory can then fail in two distinct ways: it can fail to re-emit a photon at all, or it can re-emit a photon whose quantum state has imperfect overlap with the photon that was to be stored. This motivates the distinction between efficiency (probability to emit a photon) and fidelity (overlap of the emitted photon with the original one). The latter is sometimes more precisely denoted conditional fidelity, since it is conditional on a photon having been emitted by the memory. For quantum repeater applications, for example, both efficiency and fidelity should typically be high [3], however the requirements on the efficiency tend to be somewhat less demanding than those on the fidelity. It is interesting to note that for certain ensemble-based implementations of quantum memories decoherence can affect only the efficiency without degrading the fidelity [78]. The memory performance can also be characterized by quantum tomography of the state of the emitted photon. The tomography performed via a homodyne measurement is a deterministic process which produces a full characterization of the memory, from which efficiency and fidelity can be extracted.

3.2 Memories for general states of light

One may also have the goal of storing general states of light independently produced by a third party. Possible applications range from linear optics quantum computing to complex quantum communication protocols. Following the storage of the state, the memory can either be measured in some basis, or for other applications retrieved onto another light pulse. Various types of states can be useful here, such as coherent states, squeezed states, Schrödinger cat states, single photon, or Fock states. The characterization of the memory performance can then be done either by quantum tomography of the atomic state or by quantum tomography of the retrieved state of light[31]. Here again homodyne measurements on light are used and thus one important concept is the (unconditional) fidelity [30].

3.3 Memories that emit photons and whose state can be measured directly

A different approach to quantum repeaters, but also to the implementation of a loophole-free Bell test, cf. previous section, involves memories (for example, single trapped atoms) that emit photons which are entangled with the memory, and where the atomic state is detected directly [32,33,35,34]. The atomic state detection is typically a deterministic process, so the distinction between efficiency and fidelity does not apply in this case, the appropriate concept is (unconditional) fidelity.

3.4 Memories that emit photons and that are measured via retrieval

Even though they were not represented in QAP, we would like to mention ensemble-based memories of the DLCZ (Duan-Lukin-Cirac-Zoller) type [21] where memory excitations are created through the emission of a photon, but where the final readout of the memory is done via conversion of the memory excitation into a single photon. Memory performance can then be characterized in analogy with section 3.1 [3,7].

4 Criteria for assessing quantum memory performance

We now discuss a number of evaluation criteria (figures of merit) and their relevance for different applications and implementations.

4.1 Fidelity

In general terms, fidelity is related to the overlap between the quantum state that is written into the memory and the state that is read out. It should be noted that the

definition of fidelity that is typically used in the context of quantum memories is different from the fidelity used in quantum information theory, e.g. in the context of unambiguous state discrimination, Uhlmann's theorem etc. [38]. For two pure states, the latter corresponds to the modulus of their overlap, whereas the former is the square of that modulus.

The precise operational meaning of the fidelity depends on the specific approach. For memories that store and re-emit single photons, the fidelity is defined as the overlap between the single-photon wave packet that was sent in and the one that is recovered from the memory. This is also denoted *conditional fidelity*, because it is conditional on the re-emission a photon. The probability to actually recover a photon is denoted *efficiency*, cf. the next subsection. For memories that are meant to store general states of light, the conditional fidelity is not an appropriate concept, and one has to consider *unconditional* fidelities.

Note that for some applications, the purity of the output state (for a pure input) can be a better criterion than the fidelity. If the output state is related to the input state by a unitary transformation, this may do no harm. For example, a Bell measurement involving two photon wave packets [36] that have both been stored in quantum memories can be performed with high accuracy if both wave packets have been subject to the same unitary transformation (distortion). However, it seems that impurity of the output state would be a problem for most conceivable applications in quantum information. Such impurity could have different forms, depending on the implementation (e.g. timing jitter, depolarization).

It is clearly important to study which processes will limit the fidelity (purity) of a given implementation. It is also interesting to study which encodings of quantum information are the most advantageous in a given physical system (are there "decoherence-free subspaces"? [37]).

4.2 Efficiency

We already introduced the concept of memory efficiency in the previous section. It is most clearly defined for the case of memories that are meant to store and emit single photons, where it is the probability to re-emit a photon that has been stored. In atomic ensembles the efficiency can in principle be close to one thanks to collective interference effects. For single atomic systems (including quantum dots and NV centers), the efficiency with which a single emitted photon can be recovered is typically small, but it can be enhanced through the use of optical cavities. Efficiency is not a well-defined concept for memories that are meant to store general states of light, the use of (unconditional) fidelity is usually more appropriate.

It is interesting to note that, while high recall efficiency is clearly desirable, it is not always necessary to be very close to 100 % for the memory to be useful, for example for proof-of-principle demonstrations of quantum repeaters. However, some applications, such as teleportation of an unknown state, require that the storage of a light state in the memory has unconditional high fidelity.

In other words, the combined fidelity times efficiency must be higher than the classical limit. It is important to study the efficiency required for different applications, see e.g. Ref. [3] for quantum repeater requirements.

4.3 Storage time

This is clearly very important for long-distance quantum communication applications, where the communication time between distant nodes imposes a lower bound on the required storage time. Storage times have to be at least as long as the average entanglement creation times, which are at least in the second range for realistic repeater protocols and relevant distances [3]. A quantitative study of the effect of storage time limitations was recently performed in Ref. [39]. Long storage times are less important for other applications such as single-photon sources or loophole-free Bell tests.

4.4 Bandwidth

This will influence the practical usefulness of a given memory for most applications, because it determines the achievable repetition rates, and also the multiplexing potential, cf. below. Bandwidth considerations can also be important for matching sources (e.g. parametric down-conversion) and memories. Of course the required numerical value will depend on the desired application.

4.5 Capacity to store multiple photons and dimensionality

The capacity to store several modes is a natural capability for certain ensemble implementations, which can allow a multiplication of the repetition rate, e.g. in quantum communication [28,40]. It is then of interest to quantify the maximum number of photons (modes) that can be stored. The criterion does not apply to single-atom approaches in the same way. The ability to store multiple spatial modes, i.e. to generate quantum holograms, which is inherent to atomic ensembles is one exciting perspective [41]. For a single-mode memory, it can be interesting to quantify its dimensionality, i.e. how many excitations (photons) can be stored.

4.6 Wavelength

As mentioned above, for long-distance quantum communication applications it is important that the wavelength of the photons that propagate over long distances is within the region of small absorption in optical fibers (unless one considers free-space transmission, e.g. to satellites). Depending on the protocol under consideration, this may constrain the operating wavelength of the respective quantum memory.

5 Physical Requirements

In this section we want to focus on the physical requirements for implementing good memories, where "good" is defined with respect to the figures of merit discussed in the previous section. We will focus on figures of merit that seem particularly important, and that are relevant for all approaches, namely efficiency and/or fidelity, and storage time. The described criteria are generally not independent. For example, the longer the desired storage time, the harder it may become to achieve high efficiency and/or high fidelity.

We suggest that for any memory protocol there are at least two requirements in order to achieve high efficiency/fidelity and significant storage time, namely good coupling between traveling and stationary excitations, and good coherence.

5.1 Light-matter coupling

The notion of light-matter coupling is most easily defined for memories that operate by absorbing and re-emitting states of light (cases 2.1 and 2.2 above). In this case, the notion of coupling is directly related to the probability of absorbing the light. In the case of atomic ensembles (whether in gaseous form or in solids), good coupling is achieved by having high optical depth. If such a memory is realized by a single quantum system inside a high-finesse cavity, for example, then the finesse of the cavity will play a role that is analogous to the optical depth. For memories where the memory excitation is created via the emission of a photon (cases 2.3 and 2.4), a critical point is the probability to emit this photon into a well-defined mode. It is at this point that the notion of good coupling intervenes in such systems. For case 2.4, it is also important in the readout process.

Optical depths that are sufficient for excellent memory performance have already been achieved in atomic gas cells (both hot and cold), and are in the process of being achieved for rare-earth doped crystals, using multi-pass configurations and/or particularly strongly absorbing materials. High unconditional fidelity furthermore requires good coherence and high detection efficiency (for the homodyne detection), which have both been achieved in experiments in Copenhagen (see section 6.5). For individual systems such as trapped atoms and NV centers efficient collection of the emitted photons could be achieved with high-Q cavities. It is also worth noting that the possibility of storing multiple modes (temporal, spatial, directional) is being investigated in several ensemble-based approaches. These points will be discussed in detail in section 6.

5.2 Coherence

We also discuss decoherence. Its effects can be different for different approaches. For example, for memory protocols based on collective effects, such as controlled reversible inhomogeneous broadening (CRIB), decoherence affects the efficiency, but not the conditional fidelity. On the other hand, for single atoms decoherence primarily affects the fidelity, but not the readout or recall efficiency. Nevertheless, decoherence is an important consideration for all implementations. In most systems the coherence is limited by fluctuating magnetic fields. These can be externally applied fields (for trapped atoms) or fields generated by the solid-state environment, in particular nuclear spins in the host material (NV centers, quantum dots, rare-earth ion ensembles). Coherence properties can then be greatly improved by optimizing the choice of host material (e.g. isotopically purified crystals that have very low concentration of nuclear spins). The following section develops the described topics in more detail for the different experimental approaches within QAP.

6 Implementations

6.1 Rare-earth ions in solids (Lund/Geneva)

We now discuss the possible realizations of quantum memories using ensembles of rare-earth ions in solids. The optical $4f$-$4f$ transitions in rare-earth ions are known for their long optical coherence times (100μs-1ms) [42,43] at cryogenic temperatures and it is also possible to find spin transitions with extremely long coherence time (> 1 second) [44,45,46]. This make them very suitable for transferring photonic quantum states onto collective atomic coherences, which can be optical as well as spin. Doped into solids the optical transitions have inhomogeneous broadening [47] much larger than the homogeneous broadening given by the optical coherence time. This causes inhomogeneous dephasing of the induced optical coherence that needs to be compensated for. We mention already that the inhomogeneous broadening offers the possibility of a large-bandwith light-matter interface.

In order to control the inhomogeneous dephasing the considered storage protocols are based on absorption and re-emission of photons using photon-echo effects. It has been shown, however, that traditional two-pulse photon echoes are not suitable for the storage of quantum light [48,49]. This is due to intrinsic spontaneous-emission noise induced by the strong π-pulse used for rephasing of dipole moments. We are going to describe two modified photon echo protocols that can in principle store single photons with efficiency and fidelity up to unity. The first protocol is based on the controlled and reversible inhomogeneous broadening (CRIB) [50,51,52,53,54,55,56,57,58] of a single absorption line (for a recent review see [8]). The second protocol is based on the reversible absorption by a periodic structure of narrow absorption peaks, a so called atomic frequency comb (AFC) [59,60,61,62,63]. Potential areas of application for this type of quantum memories are for long-distance quantum communication (quantum repeaters) and the realization of quasi-deterministic single-photon sources.

6.1.1 Controlled reversible inhomogeneous broadening

We now describe the first scheme, controlled reversible inhomogeneous broadening (CRIB) [8]. This involves broadening an initially narrow absorption line using the linear Stark effect and an applied external electric field gradient [51,52,54,57]. The width of the broadened line should match the spectral width of the light that is to be absorbed. Re-emission of the light is triggered by changing the sign of the field, which inverts the atomic transition frequencies around the central frequency. The rephasing mechanism can be understood by the following argument. Atoms at detuning Δ with respect to the carrier frequency of the light accumulates a phase $\exp(-i\Delta\tau)$ between absorption ($t=0$) and the polarity inversion of the electric field ($t = \tau$). By inverting the polarity, the atoms invert their detunings $\Delta \to -\Delta$. After a time $t = 2\tau$ the atoms will have accumulated an opposite phase factor $\exp(i\Delta\tau)$ which results in a rephasing of all atomic dipoles.

The following formula can be derived for the memory efficiency η_{CRIB} [54,64]:

$$\eta_{CRIB}(t) = (1 - e^{-\tilde{d}})^2 \mathrm{sinc}^2(\gamma_0 t), \qquad (1)$$

where $\tilde{d} = d\gamma_0/\gamma$. Here γ_0 is the width of the initial narrow line, γ is the width of the broadened line, d is the optical depth of the initial line, and t is the storage time in the excited state. Note that the initial absorption depth is decreased by the broadening factor γ/γ_0. Thus the more broadening that is added, the less efficient the storage efficiency becomes. The storage of a single pulse (one mode) can be chosen to be essentially equal to the pulse duration (and thus inversely proportional to γ). Once the pulse has been absorbed, the created atomic excitation can be transferred to a lower-lying state [51,52], e.g. a state that lies in the same hyperfine multiplet as the ground state. The storage time in such a hyperfine state is limited only by (hyperfine) decoherence, cf. below.

One can see that the total efficiency is the product of two factors. The first one is related to the absorption of the light. In fact, it is precisely the square of the absorption probability in the broadened ensemble, since is the optical depth of the broadened line. The square intervenes because in the CRIB protocol, the re-emission process is the exact time reversal of the absorption, so the probability is the same for both processes. The second factor (the squared sinc function) describes the dephasing which is due to the fact that the initial narrow line has a finite width γ_0. The exact form of the last factor depend on the shape of initial line (which we here assume to be a square function), it being related to its Fourier transform.

In Ref. [28] an analysis of the performance of CRIB was performed, particularly in terms of multimode storage. It was found that an optical depth of about 30 is required to achieve an efficiency of 0.9 for the storage of a single pulse (one mode). If larger optical depths are available, one can store multiple temporal modes (trains of pulses), which can be very attractive for certain applications, e.g. quantum repeaters. The number of modes that can be
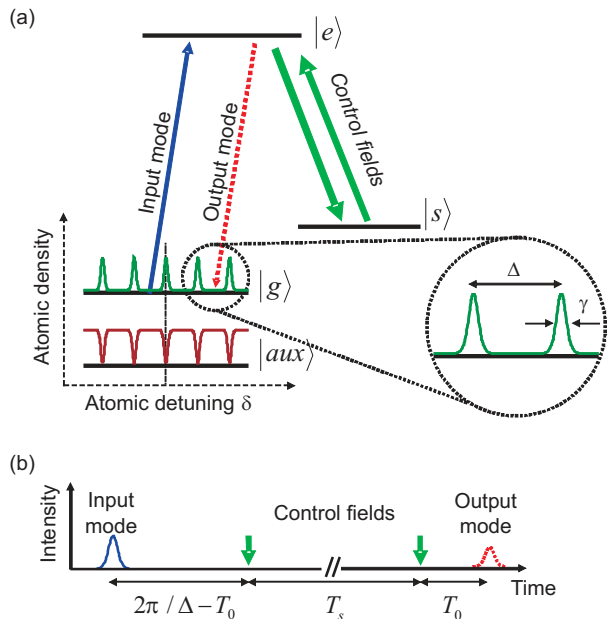

Fig. 1. The AFC quantum memory scheme. Figure from Ref. [59].

stored with a certain fixed efficiency grows linearly with the optical depth [28,65].

6.1.2 Atomic Frequency Combs

In order to fully exploit temporal multiplexing in quantum repeater architectures, the memory should be able to store many temporal modes with high efficiency [28]. For EIT based quantum memories, this requires extremely high and currently unrealistic value of optical depth [59,65]. The scaling is better for CRIB based quantum memories but the required optical depth are still very high (e.g. 3000 for 100 modes with 90% efficiency) [28,65]. Recently, a new scheme was proposed [59] for inhomogeneously broadened materials, where the number of stored modes does not depend on the initial optical depth d. The scheme is based on atomic frequency combs (AFC).

The idea of AFC is to tailor the absorption profile of an inhomogeneously broadened solid state atomic medium with a series of periodic and narrow absorbing peaks of width γ_0, height d and separated by Δ (see Fig. 1). The single photon to be stored is then collectively absorbed by all the atoms in the comb, and the state of the light is transferred to collective atomic excitations at the optical transition. After absorption, the atoms at different frequencies will dephase, but thanks to the periodic structure of the absorption profile, a rephasing occurs after a time $2\pi/\Delta$ which depends on the comb spacing. When the atoms are all in phase again, the light is re-emitted in the forward direction as a result of a collective interference between all the emitters.

In order to achieve longer storage times and on-demand retrieval of the stored photons, the optical collective excitation can be transferred to a long lived ground state

before the re-emission of the light. This transfer freezes the evolution of the atomic dipoles, and the excitation is stored as a collective spin wave for a programmable time. The read out is achieved by transferring back the excitation to the excited state where the rephasing of the atomic dipoles takes place. If the two control fields are applied in a counterpropagating way, the photon is re-emitted backward. In that case, it has been shown that the re-absorption of the light can be suppressed thanks to a collective quantum interference. In that configuration, the theoretical storage and retrieval efficiency, assuming that the decoherence in the long lived ground state is negligible and a perfect transfer, is given by [59]:

$$\eta_{AFC} \approx \left(1 - e^{-\tilde{d}}\right)^2 e^{-\frac{7}{F^2}} \qquad (2)$$

where $\tilde{d} \approx d/F$ is the effective optical depth and $F = \Delta/\gamma_0$ is the finesse of the AFC. Note that this formula applied to a series of Gaussian peaks. In Ref. [61] a formula for Lorentzian line shapes is also given. In the equation above we see that η_{AFC} tends towards unity for sufficiently large d and F. Note that the interpretation of the efficiency formula for AFC is identical to the one for CRIB discussed above. The difference lies in the origin of the effective absorption depth $\tilde{d}$, which for CRIB is due to the applied broadening while for AFC it is due to the removal of atoms when creating the comb structure.

The number of temporal modes N_m that can be stored in an AFC quantum memory is proportional to the ratio between the storage time in the excited state $2\pi/\Delta$ and the duration of the stored photons, which is inversely proportional to the total AFC bandwidth $\Gamma = N_p\Delta$, where N_p is the total number of peaks in the AFC. Hence, we see that N_m is proportional to N_p and is independent of the optical depth. See [59] for a more detailed discussion on the multimode capacity.

6.1.3 Crystal properties

The optical depth of a given rare-earth doped crystal is proportional to the dopant concentration (for low concentrations) and to the transition dipole moment. Above a certain dopant concentration, however, adding more ions does not increase the optical depth any further [66], because ion-ion interactions lead to increased inhomogeneous broadening without changing the spectral density of absorbers at any given frequency. Furthermore the optical coherence time may decrease for higher concentrations [67], equally due to ion-ion interactions. Of course, the optical depth can also be increased by using longer crystals, or, more significantly, by using multi-pass configurations or optical cavities.

At low temperature (T=1-4 K) the optical and hyperfine coherence times are limited by the spin-spin interaction of the ions between themselves, and with spins in the host crystal [42,43]. This has led to the use of crystal hosts with low nuclear spin density, most notably Y_2SiO_5. The commonly used ions Praseodymium (606 nm), Europium

(580 nm) and Thulium (793 nm) have quenched electronic spins, resulting in weak spin interaction in general. For Erbium (1530 nm) and Neodymium (880 nm) doped crystals, however, one has to take the (much larger) electronic spins of Er and Nd into account, which will interact both with nuclear spins in the host and among themselves. Nevertheless, optical coherence times of a few ms have been demonstrated for Er-doped [68] and Eu-doped Y_2SiO_5 [66] (hundreds of microseconds for Nd and Pr in the same host [68]), while for Pr:Y_2SiO_5 hyperfine spin coherence times as long as 1 second have been reported [44,46].

In order to perform the spectral shaping of the inhomogeneous absorption profile, which is necessary for both CRIB and AFC, one uses optical pumping [69,70,71,72]. The optically pumped ions are stored in a ground state, normally a spin level with a long population lifetime. Both the CRIB and AFC protocols also use another spin-level for storing the excitation on long time scales ($>10 \mu$s) [50, 51,52,59,63]. In the preparation of the memory this level must be emptied of population, also via optical pumping. Thus, the material must have at least 3 spin levels for implementation of the complete schemes. In materials with only 2 spin levels one uses a level for population storage in the spectral shaping process, and the light is only stored in the optically excited state.

6.1.4 Experimental state of the art

The first proof of principle demonstration of the CRIB scheme with bright coherent states was realized in a Europium doped solid [53]. The Europium ions doped in the solid state matrix have an optical transition at 580 nm, and a level structure with three hyperfine states in the ground and excited states. The authors used optical pumping techniques to create a narrow absorption peak with a width of 25 kHz, within a 3 MHz wide transparency window. The absorption of the peak was approximately 40 %. This peak was then broadened with a gradient of electric field implemented with four electrodes in a quadrupole configuration, thanks to the linear Stark effect. An incoming optical pulse of 1 μs was partly absorbed by the broadened spectral feature. To read-out the memory the polarity of the electric field was reversed after a time τ. After an additional delay τ, two-level Stark echoes were observed, with a decay time of about 20 μs. In another experiment, the same authors stored and recalled a train of 4 pulses [55]. They also showed that the phase information of the input pulses was preserved during the storage. In these experiments, only a very small part of the incident pulses were re-emitted in the Stark echo (between 10^{-5} and 10^{-6}). This low efficiency can be partly explained by the small absorption of the broadened peak (about 1%). In a more recent experiment, the same group demonstrated a greatly improved storage and retrieval efficiency of 15 % using a Praseodymium doped crystal, which features an optical transition with larger oscillator strength and consequently larger absorption [56]. Using a longer crystal they could achieve an efficiency as high as

45%. Very recently, a CRIB experiment has been demonstrated at the single photon level, using an Erbium doped crystal absorbing at the telecommunication wavelength of 1536 nm [58].

Storage schemes combining off-resonant Raman interaction and photon-echo rephasing mechanisms have been proposed [73,74,75]. The experiments reported in [74,76] use a Raman interaction to transfer the optical input pulse onto a spin excitation. The spin transition is artificially broadened by an external magnetic field gradient, which allows rephasing of the spin coherence using the CRIB scheme. These experiments were realized in atomic vapours of Rb and in [76] an efficiency of 41% was reached. Moreover, it was shown that using this approach multiple pulses could be stored and later retrieved in any time order.

Phase preservation properties of photon echo techniques have also been investigated for the storage of multiple temporal modes using conventional photon echoes in Er doped LiNbO3 [77,78]. This realizes a (relatively low-efficiency) memory in the classical regime. However, the results concerning the phase coherence generalize to the case of CRIB memories. The phase coherence of the memories was also studied performing an interference experiment between two spatially separated crystals [78]. The results showed very good visibility (of order 90%), which suggests that very high fidelities should be achievable with CRIB and AFC based memories in the same system. An interesting feature of these results is that the decoherence only affects the efficiency of the memory, but not its fidelity [78] (as long as background fluorescence is negligible). This is because atoms that are decohered simply do not efficiently contribute to the collective interference that produces the echo. The same principle also applies to CRIB and AFC.

The first proof of principle demonstration of the AFC protocol has been realized with a neodymium doped crystal(Nd:YVO$_4$) [60]. This experiment was the first demonstration of a solid light matter interface at the single photon level. The authors demonstrated the coherent and reversible mapping of weak light fields with less than one photon per pulse on average onto the ensemble of Neodymium ions. This experiment showed that the quantum coherence of the incident weak light field was almost perfectly conserved during the storage, as demonstrated by performing an interference experiment with a stored time-bin qubit (see Fig. 2). Finally, they also demonstrated experimentally that the interface makes it possible to store light in multiple temporal modes (4 modes). The storage and retrieval efficiency was low (about 0.5 %) in this experiment, mainly limited by the imperfect preparation of the atomic frequency comb due to the difficulty to perform good optical pumping in Nd:YVO$_4$. In a more recent experiment, [61] demonstrated improved performance in terms of efficiency (9 %) using a Thulium doped YAG crystal, also at the single photon level. The efficiency could be further improved (to 17%) by optimization of the creation of the AFC, particularly by optimizing the shape of the teeth in the AFC [79]. The efficiency has been further improved in Ref. [62], in the bright pulse regime, reaching 34% in a Pr-doped
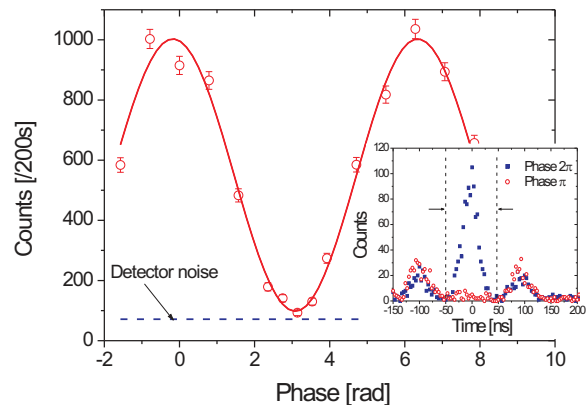

Fig. 2. Phase preservation during the storage of a time-bin qubit by an atomic frequency comb [60]. Time-bin qubits with different phases Φ, are stored and analyzed using the light-matter interface. The analysis is performed by projecting the time-bin qubit on a fixed superposition basis, which here is achieved by two partial readouts (see text for details). The inset shows the histogram of arrival times, where there is constructive interference for $\Phi = 2\pi$ and destructive interference for $\Phi = \pi$ in the middle time bin. For this particular interference fringe, a raw visibility of 82% and a visibility of 95% when subtracting detector dark counts are obtained. Figure from Ref. [60].

Y$_2$SiO$_5$ crystal. In the weak pulse regime (average photon number < 1), a storage efficiency of 25% was achieved [80]. This improvement was possible due to the ability to make narrow (100-200 kHz) peaks with high absorption depth ($d \sim 10$). The multimode capacity has also been increased by almost one order of magnitude compared to [60] in a Nd-doped Y$_2$SiO$_5$ crystal, where up to 64 modes were stored for 1.5 μs [81].

In the AFC experiments cited above, only the first part of the proposed AFC protocol was demonstrated (i.e. the coherent mapping onto collective excitation at the optical transition and collective re-emission at a predetermined time). Hence these experiments did not allow for on demand-read out. Very recently, a proof of principle demonstration of the full AFC protocol including the transfer to a long lived ground state has been demonstrated in a Praseodymium doped Y$_2$SiO$_5$ crystal [63]. True on-demand storage up to 20μs was achieved, limited by inhomogeneous spin dephasing. Spin echo techniques should allow to extend the storage time up to the spin coherence time (about 1 s) [46], even at the single excitation regime.

6.1.5 Performances

We now evaluate the expected performances of quantum storage in rare-earth doped solids with respect to the parameters proposed in the introduction.

Fidelity: Very high fidelities have been shown possible since the dominant decoherence processes affect the recall

efficiency, but not the fidelity of the output state. This is a virtue of ensemble-based quantum memories. Experiments at the single photon level has shown conditional fidelities up to 95%.

Efficiency: In theory efficiencies up to 100 % are possible with the CRIB and AFC protocols. In practice, the maximal efficiency reached so far is 45% for the CRIB protocol, and 34% for the AFC protocol, both in Pr-doped Y_2SiO_5 crystals. The challenge is to design systems with sufficiently high absorption. Another promising route towards higher efficiencies is the use of multi-pass arrangements or cavity enhanced light-matter interactions.

Storage time: Rare-earth doped solids usually feature optical transitions homogeneous linewidths of order of 1-10 kHz. Optical coherence times up to several ms have even been observed in certain rare-earth doped materials (see above). However, the storage time in the excited state is mostly limited by the width of the absorption peak γ_0. While the theoretical ultimate limit for the width of absorption peak is given by the homogeneous linewidth, in practice the narrowest peak realized so far are or order of tens to hundreds of kHz. This leads to storage times of tens of microseconds. Significantly longer storage times can be achieved if the excitation is transferred to a long lived ground state. In particular Pr doped solids have extremely long spin coherence times. Even longer spin coherence time are expected for Eu doped solids [82]. Long storage times should thus be possible.

Bandwidth: Bandwidths up to several hundreds of MHz are realistic using the atomic frequency comb protocol. The challenge is thus to find systems with sufficiently high initial absorption to achieve acceptable efficiencies. The limitation in bandwidth will in general depend on the spacing between hyperfine transitions, either in the excited or ground state. Excitation of several levels will cause quantum beat phenomena in the recall efficiency.

Multiple-photon and multiple-mode storage capacity: In principle, large numbers of photons could be stored in the same memory. Trains of wave packets can be stored. The AFC protocol is particularly promising for that aspect, since the number of temporal modes that can be stored does not depend on the available optical depth. In addition there is potential for frequency multiplexing. Limits are imposed by the storage time and the frequency bandwidth of the material. In particular, the number of modes that can be stored with the AFC protocol is proportional to the number of peaks in the AFC.

Wavelength: Rare-earth doped solids optical transitions cover a wide range of wavelengths, from 580 nm (Eu) to 1530 nm (Er). It should be noted that there is considerable flexibility concerning the operating wavelength of the photon memory in quantum repeater protocols involving non-degenerate sources of entangled photon pairs, since then photons at one wavelength can be stored in the memory, while photons at another wavelength can be sent into optical fibers. Some efficient quantum repeaters proposals however require quantum storage at telecommunication wavelengths. Erbium doped solids is the only proposed system that meets the requirements to implement a quantum memory at this wavelengths.

Read-out: For the CRIB scheme, the read-out delay for a single stored photon can be chosen at will by controlling the electric field that causes the Stark shifts used in CRIB. For the storage of multiple temporal modes, pulses stored at different times will be re-emitted at different times, thus allowing to distinguish between the modes. The order of the pulse sequence is however reversed during the storage. For the AFC scheme, the storage time in the excited state is pre-determined by the comb structure. On demand-read out can be achieved by a reversible transfer of the stored excitations to ground state level. Contrary to the CRIB scheme, the order of the pulse sequence is preserved with the AFC scheme.

Complexity: The proposed implementations uses standard lasers and fiber-optic components. The lasers are frequency stabilized to a reference for increased coherence length, which is important when shaping the absorption profile via optical pumping. The experiments also require a cryostat, operating temperatures being in the region 1-4 K.

6.2 NV Centers in Diamond (Stuttgart)

Defect centers in diamond share many similarities with the above mentioned rare earth system. Diamond defects typically comprise single or few impurity atoms in a diamond host with allowed optical transitions with absorption wavelength raging from the UV to the infrared. Those defects may be electron paramagnetic such that one can use the superior relaxation and decoherence properties of electron and nuclear spins for information storage, retrieval and processing. In contrast to rare earth systems up to now mainly defects have been studied in the context of quantum information processing that do show strongly allowed optical transitions (absorption cross section: $10^{-17} cm^2$ at $T = 300K$) such that single color centers can be observed. The popularity diamond defects have gained in quantum information over the past years is based on two aspects: On the one hand color centers in diamond usually are point defects deep within the bandgap of diamond which results in narrow and stable room temperature optical emission and excitation lines. In most cases excitation and emission without lattice phonons being involved is visible even at room temperature. On the other hand the stiff and diamagnetic diamond lattice eventually leads to very long electron and nuclear spin dephasing times, which for example can reach ms for electron spins at $T = 300 \, K$. The currently most studied defect center in diamond is the nitrogen vacancy (NV) defect (see Fig. 3).

Due to the fact that it is an electron paramagnetic system, the NV does show a set of paramagnetic electronic and hyperfine split ground and excited state levels. It thus allows for the observation of photon-spin coupling used in e.g. lambda-type optical transitions with the potential to use CRISP and AFC type of techniques for storage. Long term storage can be realized by electron and nuclear sub spin levels with very long (ms-s) coherence
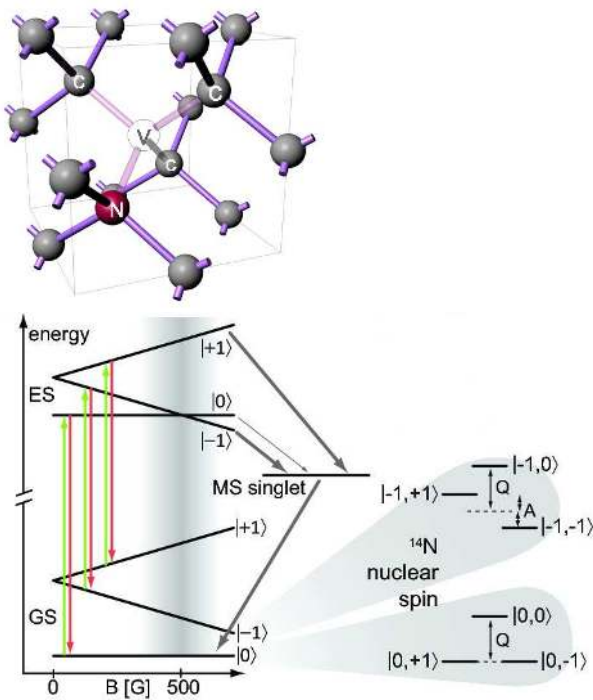
Fig. 3. In (a) a schematic picture of the NV-center embedded in the diamond lattice is shown. (b) sketches the NVs levels scheme with its possible microwave transitions and hyperfine structure as an inlay.

Fig. 4. Second-order fluorescence intensity autocorrelation function for the NV center at low temperature under resonant excitation of $m_S = 0$ spin state. The Rabi frequency of the excitation laser was varied for different curves and equals to 0.44, 0.59, 0.67, and 1.00 GHz (increase from bottom to top).

times. The NV center has a strongly allowed optical transition with a corresponding optical excitation and emission linewidth of around 10 MHz at low temperature. This enables strong defect cavity coupling to enhance the spin photon interface [83]. The project started with exploring the fundamental applicability of the NV center as a quantum storage element. Basically two lines of research were explored namely an ensemble based approach for memory based on EIT-like two-photon resonance. Secondly coupling of single photon states to single NV centers which requires efficient (strong) coupling to cavities is explored. An important requirement prior to memory application is a detailed understanding of the involved energy levels as well as the excitation dynamics and photon properties of the NV center. Fig. 3 shows the energy levels of the defect important for photon absorption and emission as well as for electron spin physics. The optical excitation path from the electron spin triplet ground state to the excited state orbital doublet allows for electron spin state conserving as well as spin flip transitions. If a transition is of lambda type (spin flip transition) or not can be determined by an external control parameter, e.g. transition wavelength or an external electric field. The existence of lambda transitions has been proven in electro-magnetic induced transparency type of experiments [84]. These experiments also demonstrate that optical excitation can be used to generate long lived ground state spin coherence, an important prerequisite for quantum memory applications. A slightly different but key observation connected to quantum repeater application as well as light source of
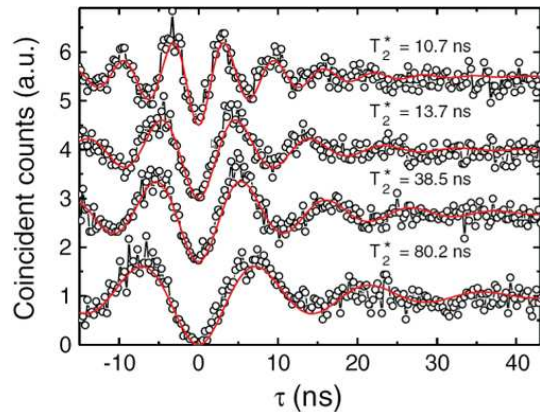
linear optical quantum information processing is the fact that single NV defects do emit transform limited photons [85] (see Fig. 4). To enhance spin-photon coupling single defect centers have been coupled to plasmonic structures [86]. Besides mere storage of photons via spin state coherence, single defects in diamond also do possess the capability to process the information stored. This particularly useful property allows for e.g. entanglement purification in quantum repeater applications. Information processing uses ^{13}C or nitrogen nuclei coupled to the electron spin of the NV center. Coherence swapping between electron and nuclear spins, entanglement among spins and basic quantum gates have been demonstrated [87]. It has been estimated that 5 qbits are sufficient for a full quantum repeater functionality [88]. This proposed spin cluster comprises one electron spin for spin-photon interaction and 4 nuclear spins for storage and entanglement pumping. First experiments on clusters of such size have been demonstrated in the meantime [89]. Spin-photon entanglement has also recently been achieved.

Fidelity: Fidelities for single or multiple photon storage in defect centers have not been determined up to now. However, subparts of the memory have been investigated towards their fidelity of state storage. This is particularly true for the spin memory part, i.e. swapping of coherences between electron and nuclear spin. Here fidelities as defined in the introductory part of this paper of up to 85% have been achieved [90].

Storage time: Storage time of the defect center memory is limited by the NV center T_1 or for arbitrary state storage T_2. In purified crystals T_2 for the electron spin has been measured to be ms. Ultimately information will be stored in nuclear spins with dephasing times on the order of tens of ms.

Bandwidth: Here the NV center can be used in a similar way than the rare earth systems in CRISP and AFC methods. A crucial part of these schemes is the possibility to create and reverse inhomogeneous broad-

ening. In the case of the NV center this can be done by inverting a magnetic field or more importantly by the recently demonstrated Stark-shift frequency tuning [91] allowing frequency multiplexing.

Wavelength: The NV center emission wavelength is centered around 700 nm and hence not in the telecommunication range. Nevertheless free space quantum communication was demonstrated with NV defects (637 nm) [92]. Emission at longer wavelength is achieved with different defect centers. Other defects in diamond like NE8 (emission wavelength 800 nm) might be more suitable for fiber-based systems [93]. In addition to this defect, 90% of oscillator strength is concentrated in zero-phonon transition of NE8 defect (compared with 10% for NV defect). Currently however, little is known about the spin states of this defect and their coherence properties.

Complexity: For storage of single photons in defect center cavity systems first steps have been taken. As mentioned in the introductory part strong coupling between single defect in diamond and the whispering gallery mode of silica micro resonator was shown. The development of other cavity system is in its beginnings. However progress was reported on NV center photonic band gap cavity coupling as well as NV center-plasmon coupling. Owing to the low electron phonon coupling diamond-based photonic memory can be operated at relatively high temperatures (up to 20 K).

6.3 Semiconductor nanotechnology (Toshiba/Bristol)

Semiconductor quantum dots could potentially be used to produce fast and efficient quantum memories to be utilised in future quantum networks or as quantum repeaters. Semiconductor based systems are compact, robust and easy to integrate with existing technology. The energy structure of the quantum dots can be engineered by manipulating the material, size, and strain. Furthermore, the well established techniques to produce high-Q cavities in semiconductor material makes it possible to achieve a high efficiency [94].

In our approach we are using a single InAs quantum dot embedded in GaAs to store and deterministically re-emit a single-photon state. The operation of the device as described in [95] is illustrated in Fig. 5 (a). The quantum dot is placed in the intrinsic region of a diode structure and biased so that the heavy-hole tunnelling rate is higher than the radiative recombination rate. On the negative side of the diode an AlGaAs barrier prevents the electron from leaving the dot. The polarisation of an incoming circularly polarised photon is transcribed to a pure spin state of an exciton confined in the quantum dot. The hole immediately tunnels out while the electron remains, thus storing the spin state. At a later time a pair of heavy-holes is returned by applying an ac voltage pulse. The positively charged exciton that is formed subsequently recombines, recreating a photon with a polarisation defined by the spin-state of the stored electron. Fig. 5 (b) shows the delayed emission for storage times up to 1 μs. The storage
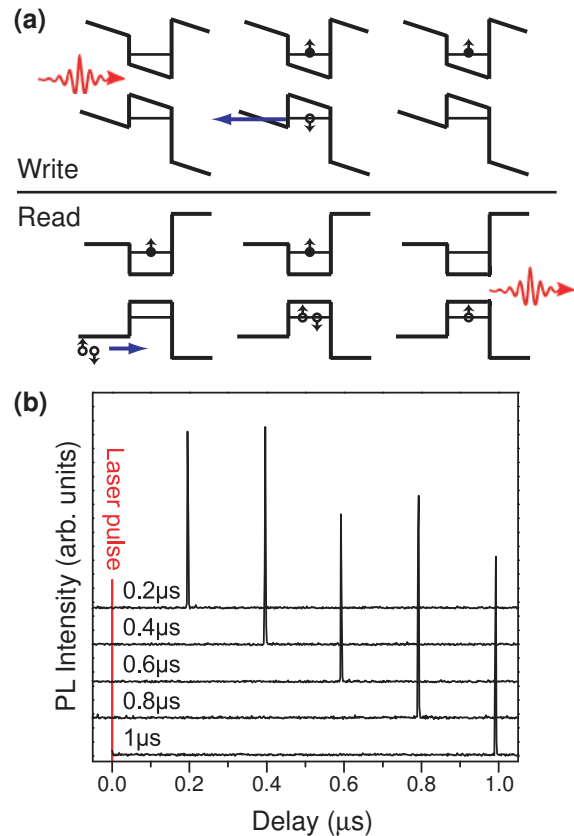

Fig. 5. (a) Schematic diagram of the quantum dot band structure and the memory scheme for pure spin storage. Write mode: A circularly polarised photon is absorbed and creates an exciton, the device is biased to remove holes (open circles), the polarisation is stored in the spin-state of the confined electron (filled circles). Read mode: The device is biased to return a pair of holes, radiative recombination results in a photon with a polarisation dictated by the stored electron's spin state. (b) Time-resolved emission from the quantum dot for readout delay times between 0.2 and 1 μs (as labeled).

time is limited by the voltage pulse pattern generator and not the device, no decrease (other than statistical fluctuations) in the readout intensity can be observed on this time scale.

Fidelity: The fidelity for the pure spin storage described above was 80 ± 10 % and constant within the delay times. This is consistent with the spin relaxation time for similar spin memories which has been shown to be in the ms range [96]. Fig. 6 (a) shows the spectrum of the delayed emission after 1 μs storage of a right-hand circularly polarised photon. The spectrum is measured both in the right- (R) and left-hand (L) polarisation basis to illustrate the high fidelity of the readout. Fig. 6 (b) shows the same measurement for storage of a left-hand circularly polarised photon.

In order to store a superposition state both the electron and hole must be retained (as their spin states are entangled), this can be done in separate reservoirs. In this case the fidelity is limited by the hyperfine interaction between the stored electron and the nuclei of the atoms

which form the quantum dot (and those in the material surrounding the dot, depending on the extent of the electron's wavefunction). For the hole, which has a p-like orbital with almost no overlap with the nuclei, the hyperfine coupling is very small. The nuclear spins give rise to a randomly fluctuating magnetic field which causes the electron spin to pick up a random phase and thus the electron spin-coherence decays with time. For III-V semiconductor material (such as the InAs-GaAs system discussed here) the decoherence time can be expected to be of the order of 10 ns.

To demonstrate coherent storage we have created an entangled exciton-photon state in a quantum dot, and observed the coherent evolution of the spin-superposed state in a dot for up to 2 ns, with a single qubit fidelity of up to 94 % [97]. The entangled exciton-photon state was prepared through the radiative decay of a biexciton in a single quantum dot. Polarisation selection rules dictate that radiative decay will project the system into the entangled exciton-photon state $\Psi \propto (|H_{XX}X_H\rangle + e^{iS\tau/\hbar}|V_{XX}X_V\rangle)$ where H_{XX} and V_{XX} are the vertically and horizontally polarised photon states and X_H and X_V are the exciton spin states coupling to the horizontally and vertically polarised photons respectively. S is the spin splitting of the stored exciton state. Fig. 6 (c) shows the measured fidelity, f^+, of the exciton-photon state to the symmetric Bell state $\Psi^+ = (|H_{XX}X_H\rangle + |V_{XX}X_V\rangle)/\sqrt{2}$, as a function of the storage time. Strong oscillations are observed as a function of the storage time with a period of h/S. The increasing phase acquired by the stationary qubit causes the final entangled photon pair state to periodically overlap with the symmetric Bell state. No loss of coherence is resolved for the longest recorded storage time of 2 ns which is limited by the radiative lifetime of the exciton. We stress that when the qubit pair fidelity is low, entanglement still exists in the system but with high fidelity to other Bell states.

Although the spin dephasing time is in the 10 ns range for III-V semiconductors, where the naturally occurring isotopes of the constituent materials all have non-zero nuclear spin [98], the nuclear field fluctuates on a much slower time scale, on the order of 100 μs. This means that a spin echo technique could be employed to extend the coherence time to this range [99]. Another alternative is to polarise the nuclear spins by optical pumping to keep the nuclear field fixed in time. Thereby any uncertainty in the phase evolution of the electron spin would be removed [100,101]. It should also be mentioned that other material systems exist where most of the nuclei are zero spin isotopes. An example of such a material system is CdSe QDs embedded in ZnSe [102].

Efficiency: For this memory scheme the input and output coupling efficiency for the photon to dot-confined exciton are similar and they predominantly determine the efficiency of the memory as a whole. Strong coupling between optical and exciton modes has been demonstrated by integrating quantum dots into optical cavities. To achieve strong coupling, the exciton-photon coupling parameter g must meet the criteria: $g^2 > (\gamma_c - \gamma_x)^2/16$ [103], where γ_c
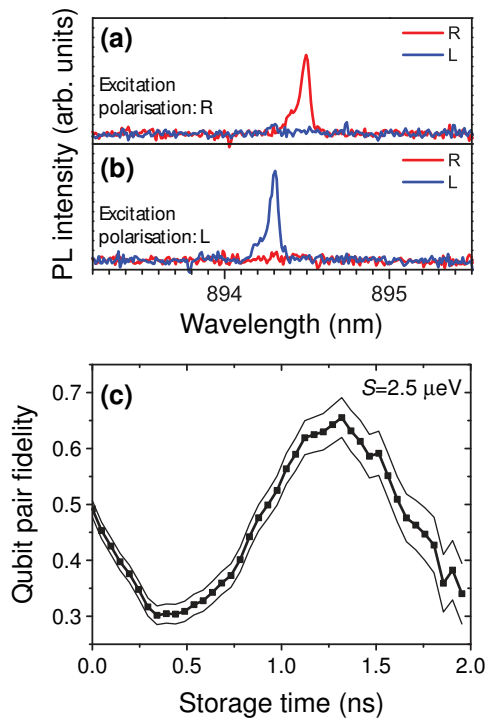

Fig. 6. (a) and (b) The spectrum of the delayed emission after 1 μs storage of a right- and left-hand circularly polarised photon respectively. The spectrum is measured in the in the right-(R) and left-hand (L) polarisation basis. (c) Coherent time-evolution of the fidelity, f^+, for the exciton-photon state with the symmetric Bell state. Bands denote measurement errors dominated by Poissonian counting noise.

and γ_x are the full width at half maxima of the cavity and exciton modes respectively; thus to reach the strong coupling limit it is necessary to fabricate cavities with very high quality factors (Q) to make the width of the cavity mode comparable to the exciton's mode. Pillar microcavities formed by etching through distributed Bragg reflectors, two-dimensional photonic crystals and microdisks have all been used to show strong exciton-photon coupling [103,104,105]. Such systems should be capable of providing near deterministic single photon absorption and emission which is required for a useful quantum memory. Our best output coupling efficiency for microcavities is 20%, a similar input coupling efficiency should in principle be achievable. To our knowledge the best quantum efficiency achieved for exciton-cavity mode coupling between excitons in quantum dots and a microcavity is 97 % [106]. We have been working to extend strong coupling schemes to show the possibility of a deterministic photon-spin quantum interface using charged dots [107]. A singly charged quantum dot, when spin polarised will interact differently to different circular polisation states of light due to Pauli blocking. When this occurs in a strongly coupled QD-cavity system the spin state of the charged dot induces giant circular birefringence and giant optical Faraday rotation. This enables non-demolition measurement of single spins, entanglement between a spin and a single photon and the development of various photon-

spin, photon-photon and spin-spin entangling gates. As a result this could provide an efficient read-in, read-out quantum memory and quantum relay. As yet no experimental demonstration has been reported.

Storage time: The limiting factor here will be the decoherence time of the electron spin stored in the quantum dot (which could be $> 100\mu s$).

Bandwidth: The bandwidth will be limited by the speed at which the gates controlling the device can be operated, hole tunnelling times, and the exciton's radiative lifetime. The latter is usually around 1 ns for an isolated quantum dot but can be greatly reduced for a quantum dot in a cavity by the Purcell effect. Operation at 1 GHz has been demonstrated for single photon emission from quantum dots in diodes [108].

Multiple-photon and multiple-mode storage capacity: Frequency multiplexing is possible with multiple dots of different size. Multiple photon storage in the single quantum dot scheme is not likely.

Wavelength: Initial experiments exploit the benefits of silicon detectors and work in the near-IR, around 900 nm. We have developed some quantum dot based devices at telecom wavelengths [109]. In principle the emission wavelength can be tuned arbitrarily by using appropriate materials and manipulating the quantum dot size and strain.

Complexity: Production of the quantum memories only involves standard semiconductor fabrication techniques. The operation of the quantum memory however requires liquid helium temperatures. As the temperature is increased confinement of the electron in the dot reduces as thermal activation becomes possible. This limits operation to <50 K for typical InAs quantum dots which are optically active at 900 nm. Confinement can be increased to allow higher temperature operation by altering the growth of the dots or changing the dot and/or barrier materials.

In summary, we have developed a spin memory based on semiconductor quantum dots. This was done by creating devices which provide preferential tunnelling of holes to allow a spin encoded exciton to be decomposed and the pure spin state stored by the electron confined in the dot. With this device we have demonstrated storage of pure spin states for 1 μs with a fidelity of 80 %. Furthermore, we have demonstrated that the coherence of a photon entangled with a stored exciton does not decay within the exciton radiative lifetime. We also present possible routes to improve a semiconductor quantum memory.

6.4 Single optically trapped ^{87}Rb atoms (LMU Munich)

Brief description of approach and potential applications: This approach aims at the generation of entanglement between remote atomic quantum memories useful for future applications in long-distance quantum communication like quantum networks or the quantum repeater [2]. Such applications can be realized on basis of our recently demonstrated entanglement between a single optically trapped ^{87}Rb atom and a single emitted photon

[32,114] by applying robust probabilistic quantum gates like entanglement swapping [110], based on the quantum interference of photon pairs on a beam splitter [33,117, 112]. The memory qubit is stored in the Zeeman sublevels $m_F = \pm 1$ of the $5^2S_{1/2}, F = 1$ hyperfine ground level of a single ^{87}Rb atom (localized in an optical dipole trap [111]), whereas the photonic communication qubit is encoded in the polarization state of a single photon. Transfer of quantum information from the photon onto the quantum memory can be realized for example by quantum teleportation or similarly by remote state preparation [35]. Efficient readout with high fidelity can be performed in two ways: The memory qubit can be determined by a destructive spin measurement using a fluorescence-based shelving technique [32] or by state-selective laser ionization and subsequent detection of the charged ionization fragments. Both techniques are investigated by our group [116]. Alternatively, stored quantum information can be coherently transferred back onto a photonic qubit by optically exciting the atom on a suitable dipole transition, leading to the emission of a single photon in the same spin state as the atom. The latter technique was recently demonstrated for the first time by Wilk *et al.*, where a single ^{87}Rb atom emits a single photon into the well defined spatial mode of an high-Q optical cavity [113].

For future applications of long-distance quantum communication like quantum networks, the quantum repeater [2], or quantum teleportation between distant matter qubits it is mandatory to achieve entanglement between separated quantum processors. In order to entangle two ^{87}Rb atoms at remote locations, we intend to apply the entanglement swapping protocol [110]. For this purpose, both atoms are entangled in a first step via spontaneous Raman scattering with a single photon [32] (see Fig. 7 (a)). Each of the two photons is collected via a large numerical aperture objective, coupled into a single mode optical fiber, and guided to an intermediate location. There the photons are overlapped on a 50:50 beam-splitter (BS). In case the photons are detected in coincidence in both output ports of the BS the remaining atom-atom pair is projected onto the maximally entangled spin-singlet state (see Fig. 7 (b)). First successful experimental steps into this direction – namely the demonstration of entanglement [33,117] and quantum teleportation [34] between single-ion quantum bits at a distance of 1 m – were reported recently by Chris Monroe's group.

In this contribution we focus on figures of merit which are particularly important for the generation of entangled ^{87}Rb atoms connected via optical fiber links of several 100 m length.

Efficiency: The overall success probability of the entanglement swapping protocol is given by

$$P_{At-At} = \frac{1}{4}(p\eta)^2 e^{-\alpha(L_1+L_2)}, \qquad (3)$$

where p denotes the overall collection and coupling efficiency into the optical fiber, η the quantum efficiency of the single photon detectors, and $e^{-\alpha(L_1+L_2)}$ the photon attenuation in the optical fiber links with communication distances L_1 and L_2 and absorption α. The factor
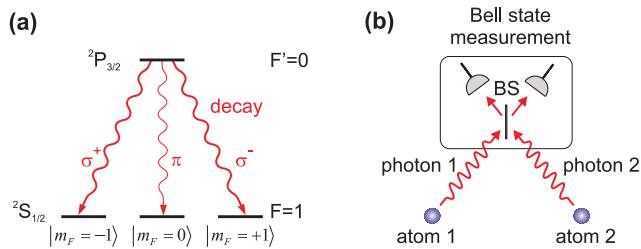
(a)

(b)

Fig. 7. (a) Preparation of atom-photon entanglement in ^{87}Rb via spontaneous Raman scattering. The atoms are excited first with short optical laser pulses to the $5^2P_{3/2}, F' = 0$ hyperfine level. In the following spontaneous emission process they decay to the ground states with the magnetic quantum numbers $m_F = -1, 0$, or $+1$ by emitting a σ^+, π, or σ^-- polarized photon, respectively. Provided these decay channels are indistinguishable in all other degrees of freedom and the π-decay is filtered out spatially a maximally entangled state is formed between the photonic qubit $\{|\sigma^+\rangle, |\sigma^-\rangle\}$ and the atomic spin-qubit $\{|m_F = -1\rangle, |m_F = 1\rangle\}$. **(b)** Preparation of a pair of entangled atoms from two entangled atom-photon pairs via entanglement swapping. The photons interfere on a $50 : 50$ beam-splitter (BS). A coincident detection of the photons in both output ports projects the atoms onto an entangled state.

4 accounts for the fact that only one out of four photonic Bell-states is detected. Typically $p\eta \approx 10^{-3}$, provided the photon attenuation is neglected. In practice we expect to achieve an overall success probability of 2×10^{-7} for the entanglement swapping process [115] via a 300 m optical fiber link. This value could be enhanced by the use of improved detection optics [119,120] or optical cavities [113], thereby allowing entanglement swapping at a higher rate.

Fidelity: When talking about fidelities (accuracies) of this scheme we distinguish in general three cases. (i) The fidelity F_{At-Ph} we are able to generate an entangled atom-photon state, (ii) the accuracy a_{det} to read out the atomic spin-state via a projective measurement, and (iii) the fidelity F_{At-At} to generate a pair of entangled atoms at remote locations via entanglement swapping. In theory atom-photon entanglement fidelities F_{At-Ph} of up to 100% are possible. However in practice due to errors in the preparation of the excited atomic state $5^2P_{3/2}, F' = 0$ the best achievable fidelity is limited to $F_{At-Ph} = 99.6\%$. To estimate now the expected atom-atom entanglement fidelity F_{At-At} after one photon has traveled e.g. an optical fiber link of 300 m length, one has to account for additional errors which are mainly due to polarization imperfections in the optical fiber [114], dephasing of the entangled atom-photon state (caused by fluctuating magnetic fields [114]), and spatio-temporal mismatch in the two-photon interference. In addition, dark counts in the single photon detectors of the Bell-state analyzer will further reduce the achievable fidelity. Applying a careful error analysis we estimate a fidelity of $F_{At-At} = 94.4\%$ to generate an entangled pair of atoms [115]. Here we emphasize that this value yet does not include the limited accuracy $a_{det} = 95\%$ to distinguish orthogonal atomic spin states via fluorescence-based shelving. Including this additional

experimental error we finally estimate an observable entanglement fidelity of $F^*_{At-At} = 81\%$ [115].

Storage time: If we scale this scenario to larger distances (several km), dephasing of the atomic spin due to fluctuating magnetic fields – respectively the resulting dephasing of the entangled atom-photon interface – will reduce the reachable atom-atom entanglement fidelity F_{At-At}. By implementing an active magnetic field stabilization and without application of any magnetic guiding field we demonstrated transverse and longitudinal spin-dephasing times of $T_2^* = 75..150~\mu s$ and $T_1 \geq 0.5$ ms, respectively, limited mainly by the residual state-dependence of the optical trapping potential and the thermal energy of the trapped atom [114]. This value is in good agreement with state-of-the-art coherence times of Zeeman qubits stored in single trapped ions. In order to achieve storage times up to several seconds one could use e.g. magnetic-field-independent hyperfine qubits and encode the photonic qubit in the frequency of a single photon [33], thereby enabling e.g. quantum teleportation between matter qubits [34] at distances of several km. Nevertheless, with the already demonstrated coherence time of $T_2^* = 75..150~\mu s$ for our Zeeman qubit an entanglement swapping experiment between two atoms connected via 300 m optical fiber can be performed in the near future.

Bandwidth: The Fourier-limited bandwidth of our single atom quantum memory is determined by the natural linewidth (6 MHz) of the dipole transition $5^2S_{1/2} \rightarrow 5^2P_{3/2}$ in ^{87}Rb. This value assures a rather uncritical implementation of the entanglement swapping protocol since the interfering photon wave packets have an overall spatial extension of several meter. In addition the temporal shape of the photons could be tuned e.g. via controlled variation of the spontaneous Raman scattering process [118] while maintaining the possibility to generate a highly entangled atom-photon interface.

Wavelength: The wavelength λ of the photonic qubit is determined by the dipole transition $5^2S_{1/2} \rightarrow 5^2P_{3/2}$ in ^{87}Rb. At $\lambda = 780$ nm the damping in optical fibers is $\approx 5..6$ dB/km. In combination with our single photon collection efficiency of $p = 4..5 \times 10^{-3}$ our current experimental implementation (two single atom traps) already allows the distribution of quantum information and entanglement between nodes of a primitive quantum network at a distance of 1 km.

6.5 Room temperature alkali gases with long spin polarization life time (Copenhagen)

Brief description of approach and potential applications: Room temperature atomic gases allow for the use of various approaches towards a quantum memory, such as Raman transitions [124] and electromagnetically induced transparency [19]. The approach we have been pursuing is based on off-resonant interaction followed by a measurement on light and a successive feedback onto the atoms. This approach is particularly suitable for room temperature atomic ensembles because it can achieve a high fidelity for the so-called symmetric atomic spatial mode, that is the mode

in which every atom contributes in the same way irrespectively of its position in the cell. For Raman and EIT based memories, a high fidelity can be achieved only for asymmetric atomic modes. The information is stored in a spin wave that is not distributed evenly over the ensemble so that atoms in the front part of the cell contribute much more to the memory than the atoms in the rear part of the cell [125]. Obviously such a memory can only have a life time that is limited by atomic motion, which is practically limited to a few tens of microseconds.

In this project we use large ensembles of up to 10^{12} cesium atoms that are kept in glass cells which are coated from the inside with a material preventing collisional decoherence. Our approach uses a quantum non-demolition (QND) type off-resonant interaction combined with quantum feedback. This has proven to work very well for the generation of deterministic entanglement of two distant objects [123], for writing a coherent state of light into a quantum memory[20], and for teleportation of a quantum state of light onto an atomic memory [127]. Potential applications include distant teleportation of atomic states and high fidelity quantum memories for light. Since high fidelity teleportation is the essential ingredient of a quantum repeater this approach is also relevant for this application.

Fidelity: The maximum obtainable unconditional fidelity of the light-to-atoms storage increases with the resonant optical depth which for a detuning larger than Doppler width is equal to the optical depth for atoms at rest. An optical depth of the order of 50 has been realized in experiments with Cesium atoms in a 25 mm long cell at a temperature close to room temperature. Fidelities of storage and teleportation up to 70% have been demonstrated experimentally for weak coherent states. For atoms initially prepared in a squeezed state the fidelity can be even higher. Such initial spin squeezing of the atoms can be achieved either by a quantum nondemolition measurement, or by preparing each atom in a coherent superposition of magnetic sublevels of the ground state. With the latter method a spin squeezing of ≈ 3 dB has been demonstrated [24].

An alternative approach to light-to-atoms state transfer is via light-to-atoms teleportation[127]. This approach has shown a fidelity of ≈ 60 %, compared to the theoretical maximum of 72%. Again, in order to improve the fidelity beyond this bound, initial squeezing should be employed, but this time the light which generates the entanglement should be squeezed. With 6 dB of squeezing, which has been demonstrated experimentally in our laboratory, a fidelity exceeding 90 % is possible.

The factors which reduce the experimentally observed fidelity below the theoretical maximum are losses of light and decoherence of atoms. Losses of light are mainly caused by reflections on the cell windows. While on the external windows' surfaces dielectric antireflection coatings can be applied easily, the internal surfaces are difficult to coat. However, it is clear that this purely technical limitation can be overcome. The atomic decoherence which is the most serious limitation to the fidelity is dominated by the decoherence caused by the driving optical field itself. At the moment this effect is responsible for the 10-15% reduction in the fidelity compared to the theoretical optimum.

Efficiency: So far our most successful quantum memory implementations involved demonstration of unconditional state transfer from light onto atoms. The unconditional character of the memory is due to the fact that the measurement on light is a homodyne measurement on a well defined spatial mode of light which can be performed with detectors with more than 98% quantum efficiency. The given fidelity is unconditional, and therefore by definition the efficiency is 100%, i.e. the process is deterministic.

Storage time: In our experiments the memory life time is defined as the time over which the fidelity drops below the classical benchmark value of 50%. Life times of up to 4 ms have been demonstrated experimentally [20]. Such a long quantum memory life time (the longest demonstrated so far for any kind of general quantum memory for light) has been made possible by using a special coating of the inside surface of the cells. With this coating atoms can withstand tens of thousands of collisions with the cell walls without loosing their coherence properties.

Bandwidth: The biggest drawback of our approach is that as of now only very narrowband light modes can be stored. The protocol relies on atoms to traverse the coupling beam many times during the write- and readout process, so that atom position effects average out. If vapour cells of a few cm^3 are used this limits the bandwidth to ≈ 1 kHz. In order to construct a photon-qubit memory using this approach, ways to design a memory which can handle a bandwidth of about 1 MHz or higher should be developed. This could be achieved with smaller cells, or with hollow fibers.

Multiple-photon and multiple-mode storage capacity: The memory can store continuous variable observables with up to a few hundred photons and therefore the dimensionality of the stored state is high. In principle, several temporal modes could be stored in the same memory using different atomic sublevels. Limits are imposed by the number of levels available.

Wavelength: The wavelength should be close to resonant frequencies of alkali atoms, i.e., 852 nm or 895 nm for Cs and 780 nm or 795 nm for Rb, to take two most popular examples. Those wavelengths are suitable for free space propagation. In order to apply this memory approach to telecom wavelengths for long distance fiber communications, the same approach can be, in principle, generalized to other systems or dual-color sources of entangled light states could be used.

Read-out delay: The limit of the read-out delay time is set by the quantum memory life time, which is up to 4 ms at the moment.

Complexity: The implementation uses room temperature atoms and therefore is simple and scalable. As for all approaches that use a great number N_a of individual physical systems to enhance the coupling between light and matter, if fields are used to perform local operations on states stored within the memory they have to be controlled precisely to $1/\sqrt{N}$. Very good magnetic shielding and low noise lasers and detectors are required to avoid technical noise.

6.6 Cold trapped atomic ensembles (Copenhagen)

Brief description of approach and potential applications: To some degree this approach is an extension of the room temperature experiments with alkali atoms: An optically dense cloud (optical depth of $\sim$15) of 10^5 Cesium atoms is prepared in one of the magnetically insensitive clock-levels by first cooling the atoms in a magneto-optical trap and successively transferring them into a far off-resonant dipole trap, which is overlapped with one arm of a Mach-Zehnder interferometer[128]. By measuring the the state-dependent phase shift that the atoms induce on probe light in the interferometer a QND interaction between light and atoms can be realized with a shot-noise and projection- noise limited precision [25].

The advantage of using a dense ensemble of cold atoms is that the sample is much smaller, light can be focused tighter and the same strong coupling can be achieved with much less photons and much shorter pulses compared to room temperature ensembles. Additionally the spontaneous scattering channels are closed, so that for similar interaction strengths QND measurements are much less destructive compared to the room-temperature vapor cell setup.

Higher optical depth can be achieved with even colder or quantum degenerate atomic samples. Utilizing condensed samples containing 10^6 Rubidium atoms stored in magnetic traps or optical dipole traps a considerable increase in coupling strength (optical depth of ~ 1000), albeit at the cost of higher system complexity, is anticipated [122]. The most promising applications for cold atom based systems are in entanglement enhanced sensing and metrology and in quantum repeaters.

Fidelity: Fidelities similar to those already obtained with atomic vapors can be expected.

Efficiency: Like in the vapor-cell experiment the efficiency of the approaches we use is 100 %, i.e. the process is deterministic.

Storage time: Quantum memory life times up to tens of milliseconds can be expected with ultracold atoms and T_2 times in this range are routinely observed for the collective coherence on the microwave clock transition. Recent investigations indicate that transversal motion of the atoms within the inhomogeneous probe beam [126] might reduce the life time of stored spin-waves, so that it might be necessary to employ an optical 3d-lattice instead of a simple linear dipole trap.

Bandwidth: Pulses of up to a few MHz bandwidth can be used. An upper limit is in principle given by the collective linewidth of the optical transition involved in the coupling scheme, so that for condensed samples also a bandwidth in the GHz range is possible.

Multiple-photon and multiple-mode storage capacity: Ensembles of 3d-trapped ultracold atoms are suitable for storage of multiple spatial modes. In principle, several temporal modes could be stored in the same memory using different atomic sublevels. Limits are imposed by the number of levels available and the level of control/compensation of external fields that cause decoherence between the different hyperfine states. For spatial multimode operation ensembles with a sample Fresnel number above 1 need to be used. To prevent mode-mixing by atomic motion, strong localization in an optical lattice is advantageous.

Wavelength: The wavelength requirements are identical to those of room-temperature atomic ensembles and determined by the atomic species used.

Read-out delay: As in the room-temperature atomic vapors the limit of the read-out delay time is set by the quantum memory life time.

Complexity: The complexity is comparatively high: the implementation uses ultracold atoms trapped in a dipole trap and requires a very low phase noise microwave source to perform LOCC operations on the stored quantum state, as explained in Sec. 6.5.

6.7 Raman memory in atomic gases and solids (Oxford)

Off-resonant Raman interactions provide a natural way to access long-lived material coherences optically, utilizing the strong light-matter coupling of an intermediate dipole transition, while avoiding fluorescent losses. Spontaneous Raman scattering has already been used to entangle separated atomic ensembles [129,130], which operation forms the basis of the DLCZ quantum repeater architecture [21]. Running the interaction in reverse offers the possibility to
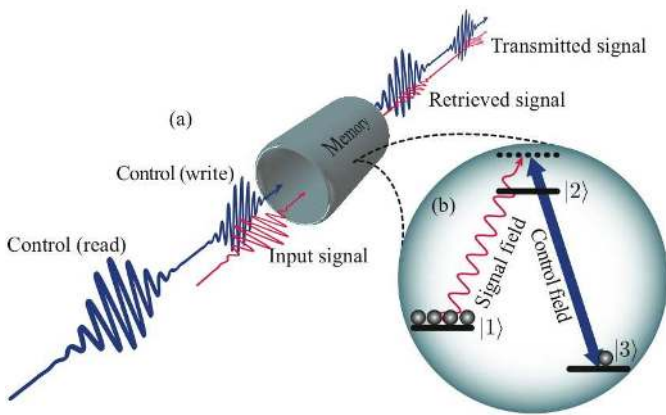
Fig. 8. (a) A Raman memory. The signal is directed into the memory along with a bright write pulse and is stored. If the storage is partial, any unstored signal is transmitted through the memory. A subsequent read pulse extracts the stored excitation, which emerges along with the transmitted read pulse. (b) The Λ-level structure of the atoms in the memory. The atoms are prepared in the ground state $|1\rangle$ by optical pumping. The signal is tuned into two-photon resonance with the control field; both are detuned from the excited state $|2\rangle$. Absorption of a signal photon transfers an atom from $|1\rangle$ into the storage state $|3\rangle$ via Raman scattering stimulated by the control. Upon retrieval the interaction is reversed.

coherently store propagating photons as stationary excitations of a Raman coherence.

Our experiments have focussed on the manipulation of temporally short, broadband wavepackets. We implemented a Raman memory for sub-nanosecond pulses in cesium vapour, and we probed the optical phonon modes of diamond via ultrafast Stokes and anti-Stokes scattering. In both cases coupling over a wide spectral bandwidth is possible because the narrowband atomic states are dressed by the application of a bright, short control pulse, producing a broad virtual state that mediates the interaction.

6.7.1 GHz optical memory in cesium vapour

Although Raman storage is well-known theoretically [124, 131, 132, 133], it has not previously been realized experimentally. Superficially it resembles EIT-based storage, except that the optical fields are detuned away from the excited state resonance (see part (b) of figure 8). Qualitatively, they operate on quite different principles: in EIT the strong dispersion associated with the quantum interference of two absorption pathways — direct or via the control field — is employed to bring a signal pulse to a halt inside an atomic ensemble. In a Raman memory the large detuning destroys this interference, and instead the signal is coherently absorbed into the virtual state created by the control pulse, with no reduction in group velocity.

In the experiment [134], a bright control pulse and an orthogonally polarized weak signal pulse, both of ~ 300 ps duration, are spatially and temporally overlapped and directed into a glass cell containing warm cesium vapour, where around 30% of the signal field is converted into a *spin wave* — a stationary excitation of the ground state hyperfine coherence. 12.5 ns later, a second control pulse extracts the stored excitation with $\sim 50\%$ efficiency, which emerges as a retrieved signal pulse. Figure 9 shows a typical time-trace of the intensity of the transmitted signal field detected by a fast avalanche photodiode placed downstream from the cell, after removal of the transmitted control field by polarization and spectral filtering. It is clear from part (b) that the bandwidth of the retrieved signal field is at least 1 GHz, but this measurement is limited by the response time of the detector, which is 1 ns. Theoretically the Raman memory operates at the full bandwidth of the control pulse of around 1.5 GHz.

Decoherence of the spin wave over the short storage time shown here is negligible; recently we observed retrieval after $\sim 2\mu$s, although some technical adjustments are required to test longer storage times. The efficiency of our memory is limited by the strength of the Raman coupling attainable, and by the quality of the overlap between the write control pulse and the incident signal. Appropriate pulse shaping (which may be technically challenging), and increasing the control pulse energy (which should not be), could raise the total efficiency to around 60% [131]. Phasematched retrieval in the backward direction allows efficiencies above 90% to be reached [135].

The memory performs reasonably well when evaluated against the criteria introduced in Section 4. The **fidelity** of the memory is (up to a possible unitary re-shaping of the retrieved pulse profile [136]) the same as the **efficiency**, which is $\sim 15\%$. As discussed above, much higher efficiencies are feasible. A proxy for the **conditional fidelity** is given by the visibility of interference between the retrieved pulse and an appropriately attenuated replica of the stored pulse. The short storage time of 12.5 ns makes this measurement relatively straightforward, and we obtained a visibility of $\sim 85\%$, after correcting for imperfections in the interferometer. Theory suggests further improvement may be possible if the Stark shift on the retrieved signal due to the strong control can be compensated.

The limiting **storage time** of the current memory is probably on the order of 100 μs; a typical coherence time in warm atomic vapours set by the diffusion of atoms out of the interaction region [137]. Longer times are of course possible if the atoms can be confined, for example by the walls of the vapour cell, although special care should be taken that the optical fields address the full cell diameter, and that collisions of atoms with the cell wall do not dephase the Raman coherence. Coherence times in warm cesium vapour on the order of 10 ms have been achieved with such a set-up by the Copenhagen group [123], with only residual magnetic fields and Cs-Cs spin exchange preventing longer coherence times. Other possibilities for extending the memory lifetime include trapping the atoms in an optical lattice [138] or   most appealing of all   as
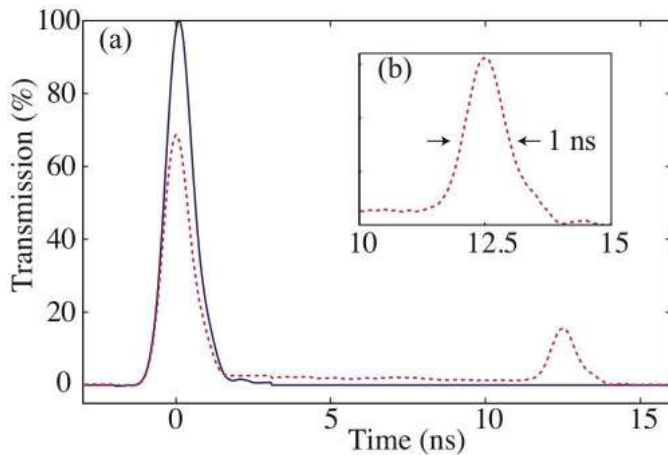
Fig. 9. Storage and retrieval of a sub-nanosecond signal pulse. (a) Solid line: Transmission of incident signal field without the presence of control field — there is no storage and no retrieval. Dashed line: In the presence of control fields (not visible) we observe 30% storage and 50% retrieval, yielding a total memory efficiency of 15%. (b) Zoom of retrieved signal field showing the measured full width at half maximum (FWHM) temporal duration of 1 ns, limited by the detector response time. This shows that the bandwidth of the retrieved signal exceeds 1 GHz.

dopants in a solid-state host (see the discussion of CRIB and AFC memories in section 6.1).

The **bandwidth** of the current memory exceeds 1 GHz, which compares favourably with the clock rates of modern classical computers. Time bandwidth products of the order of 10^5 are feasible if the full storage time is exploited. The bandwidth is limited by the ground state hyperfine splitting of 9.2 GHz in cesium, since larger bandwidth pulses will address both control and signal transitions simultaneously (this is known as the impulsive regime in the Raman literature [139]). Other media with larger splittings, or appropriate selection rules, could allow the storage of shorter pulses; the diamond memory introduced in the next section is an example.

The **multimode capacity** is not generally large — it scales poorly with the density of the ensemble, as indeed does the capacity of EIT storage [140] — although off-axis beam geometries do allow for angular multiplexing [135, 141,142]. Finally, the **wavelength** is tunable in principle, although the present memory is operated sufficiently close to resonance that significant wavelength variations away from 852 nm would rapidly erode the efficiency: the tunability is currently limited to a few GHz. Again, alternative media with sufficiently large Raman cross-sections — such as the diamond memory discussed below — can be operated far from resonance, where the Raman coupling varies slowly with frequency, allowing for near-arbitrary wavelength tunability.

Solid state memory in diamond Diamond has a very large Raman cross-section. Although its bandgap lies in the ultraviolet, optical pulses will readily scatter from
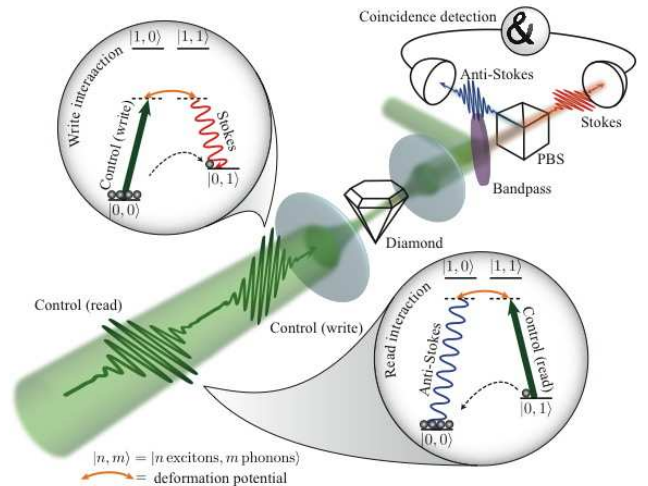

Fig. 10. Creation and detection of phonon excitations in diamond. A pair of 50 fs control pulses are focussed into a crystal of diamond. When the 'write' pulse generates a Stokes photon, a phonon is created. The 'read' pulse can then scatter from this excitation, producing an anti-Stokes photon that returns the crystal to its ground state. Coincidence measurements reveal the resulting statistical correlations arising between Stokes and anti-Stokes detection events.

the 'deformation potential', producing correlated pairs of Stokes photons and optical phonons. These phonons are non-propagating vibrational excitations associated with the 'ringing' of the crystal basis. They survive for approximately 5 ps before decaying into pairs of short wavelength acoustic phonons — sound waves — due to high order anharmonic couplings in the diamond lattice. Although this lifetime is extremely short, the optical phonons are interesting because they are very energetic, with a Stokes shift of 1332 cm^{-1} (0.16 eV, or expressed as an optical wavelength, 7.5 μm). This is much larger than the energy scale associated with thermal fluctuations at room temperature, so these excitations are naturally isolated from noise. Additionally, the large splitting allows Stokes photons to be spectrally distinguished from the control field used to initiate the interaction, even if their spectra span 10s of nanometers. Therefore, ultrashort, femtosecond timescale pulses can be used to address the phonons: on such timescales the coherence time of the phonons appears long!
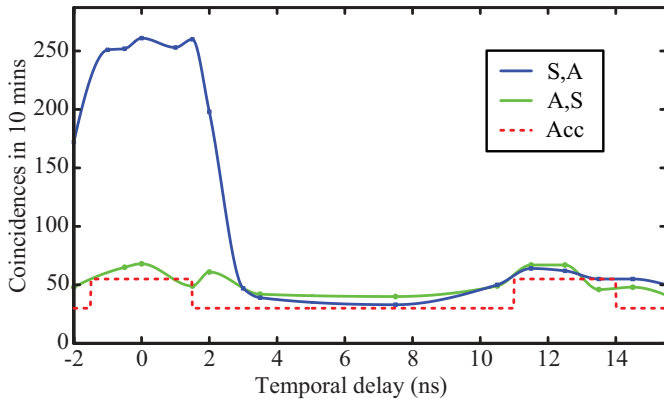
Fig. 11. Read out of phonons in diamond, as revealed by examining the correlation between Stokes and anti-Stokes detection events. The green curve shows the coincidence rate associated with the 'wrong' detection order (A,S), in which an anti-Stokes photon is scattered from the write pulse and a Stokes photon scatters from the read pulse. Photons scattered from the write and read pulses are distinguished by their polarizations. The blue curve describes the correlations for the 'correct' ordering (S,A). No significant correlations are observed for the incorrect ordering (although the polarization selection rules in diamond are not perfect, so there is a residual contribution from the correct ordering). The correct ordering exhibits a pronounced peak around zero delay. This peak is a signature that phonons are created by the write pulse and read out by the read pulse from the same control pulse sequence — the 5 ps delay between the read and write control pulses is not resolvable. Subsidiary maxima occur for delays that are multiples of 12.5 ns, which is the laser repetition rate. These are spurious, being a symptom of the increased accidental coincidence rates associated with a pair of independent control pulse sequences (dashed red line, calculated for a 3 ns coincidence gate, with reasonable technical noise).

The optical phonons in bulk diamond represent a unique testbed for the ultrafast control of macroscopic coherence in solid state systems at room temperature. As an extension of previous work [143,1] in atomic vapours to such systems, we adopted the goal of generating, and then verifying, entanglement between the phonon modes of two separated diamond crystals. We have successfully taken the first step in this direction, namely demonstration of the ability to create and detect phonons.

Figure 10 shows the experimental arrangement used, along with the structure of the interactions involved. In figure 11 the Stokes/anti-Stokes coincidence rate is plotted as a function of an electronically introduced time-delay between the two detection events. The surge in correlations around zero delay is attributed to the survival of phonons over the (unresolved) period separating the control pulses.

The next stage of these experiments is to interfere the Stokes modes from a pair of diamond crystals, so as to erase the *welcher weg* information about the origin of a detected Stokes photon. Such a detection then entangles the phonon modes of the crystals; subsequent application of read pulses to the crystals transfers this entanglement back to the optical domain, where it can be witnessed by

interfering the anti-Stokes modes. The scheme is identical to that implemented in [144,143,129], except that the entanglement is created in a solid, a technical challenge being that is survives for a time that is too short to be resolved electronically.

Although the current experiments with diamond are not focussed on the realization of an absorptive optical memory, the planned entanglement generation set-up can be adapted to function as a post-selected memory [143], which is prepared by the Stokes detection that heralds entanglement. From this perspective, it is interesting to evaluate the performance of diamond as a memory by the criteria introduced in Section 4.

For storage of a polarization qubit, the **fidelity** can be high in principle, being limited only by the stability of the set-up and the coherence time of the memory. The retrieval probability is generally low, which translates into low **efficiency**, although this could be mitigated by boosting the energy of the read pulse. The **storage time** of 5 ps is extremely short — far too short to find applications in any quantum communication protocols. It is possible, however, that it could be of use as a solid-state register, as part of a miniaturized integrated quantum processor.

The **bandwidth** is extremely large, being on the order of tens of THz. This allows the storage of ultrafast pulses, a million times shorter than any other memory has so far demonstrated. The time bandwidth product for the memory is accordingly on the order of 1000, despite its short coherence lifetime.

The **multimode capacity** of the memory is probably small, for the same reasons as discussed above in the case of an absorptive Raman memory. Nonetheless, as with all ensemble memories, spatial or angular multiplexing could be used. Finally the **wavelength** is extremely tunable, since diamond is transparent to all optical frequencies, with a Raman cross-section that varies little over the visible or telecoms spectra. Essentially any choice of wavelength is viable.

7 Summary and Outlook

Fig. 12 summarizes where the different approaches position themselves with respect to the applications discussed in section 2 and to the criteria discussed in section 4.

The experimental projects in this review are in different stages in their development. Some have already demonstrated quantum features such as entanglement with light or realized quantum protocols such as teleportation. Others are in an earlier stage. All approaches appear to be suitable in principle for high-fidelity and high-efficiency operation. The technological challenges that have to be overcome to this end vary between the different approaches. Most implementations aim for bandwidths in the range 100 MHz to 1 GHz and for storage times in the ms to s range. Concerning complexity, most solid-state implementations require cryostats and some micro- or nanofabrication, while atomic approaches tend to require laser cooling and trapping.

In the future it will be interesting to investigate various ways of combining the different approaches discussed here. Recent examples for this trend include the combination of continuous-variable and single-photon concepts in the context of quantum repeaters [145], and a proposal for creating entanglement between a trapped ion and a quantum dot [146].

References

1. H.J. Kimble, Nature **453**, 1023 (2008).
2. H.-J. Briegel, W. Dür, J.I. Cirac, and P. Zoller, Phys. Rev. Lett. **81**, 5932 (1998).
3. N. Sangouard, C. Simon, H. de Riedmatten, and N. Gisin, arXiv:0906.2699, submitted to Rev. Mod. Phys.
4. E. Knill, R. Laflamme, and G.J. Milburn, Nature **409**, 46 (2001).
5. P. Kok, W.J. Munro, K. Nemoto, T.C. Ralph, J.P. Dowling, and G.J. Milburn, Rev. Mod. Phys. **79**, 135-174 (2007).
6. A.I. Lvovsky, B.C. Sanders, and W. Tittel, Nat. Phot. **3**, 706 (2009).
7. K. Hammerer, A.S. Sørensen, and E.S. Polzik, arXiv:0807.3358, to appear in Rev. Mod. Phys.
8. W. Tittel *et al.*, Laser Photon. Rev. **4**, 244 (2010).
9. M.D. Lukin, Rev. Mod. Phys. **75**, 457 (2003).
10. P. Zoller *et al.*, Eur. Phys. J. D **36**, 203-228 (2005).
11. N. Sangouard *et al.*, Phys. Rev. A **76**, 050301 (2007).
12. K. Saucke, Diploma Thesis, University of Munich (2002).
13. C. Simon and W.T.M. Irvine, Phys. Rev. Lett. **91**, 110405 (2003).
14. H. Buhrman, R. Cleve, S. Massar, and R. de Wolf, to appear in Rev. Mod. Phys., arXiv:0907.3584v1.
15. D.E. Browne, J. Eisert, S. Scheel, and M.B. Plenio, Phys. Rev. A **67**, 062320 (2003).
16. N.C. Menicucci *et al.*, Phys. Rev. Lett. **97**, 110501 (2006).
17. L.P. Lamoureux *et al.*, Phys. Rev. Lett. **94**, 050503 (2005).
18. S. Lloyd, Science **321**, 1463 (2008).
19. M. Fleischhauer and M. D. Lukin, Phys. Rev. A **65**, 022314 (2002).
20. B. Julsgaard *et al.*, Nature **432**, 482 (2004).
21. L.-M. Duan, M.D. Lukin, J.I. Cirac, and P. Zoller, Nature **414**, 413 (2001).
22. J. Appel *et al.*, Phys. Rev. Lett. **100**, 093602 (2008).
23. K. Honda *et al.*, Phys. Rev. Lett. **100**, 093601 (2008).
24. T. Fernholz *et al.*, Phys. Rev. Lett. **101**, 073601 (2008).
25. J. Appel *et al.*, Proc. Nat. Acad. Sci. Americ. **106**, 10960 (2009).
26. W. Wasilewski *et al.*, arXiv:0907.2453.
27. J.A. Jones *et al.*, Science **324**, 1166 (2009).
28. C. Simon *et al.*, Phys. Rev. Lett. **98**, 190503 (2007).
29. M.U. Staudt *et al.*, Phys. Rev. Lett. **99**, 173602 (2007).
30. K. Hammerer, M.M. Wolf, E.S. Polzik, and J.I. Cirac, Phys. Rev. Lett. **94**, 150503 (2005).
31. M. Lobino, C. Kupchak, E. Figueroa, and A.I. Lvovsky, Phys. Rev. Lett. **102**, 203601 (2009).
32. J. Volz et al., Phys. Rev. Lett. **96**, 030404 (2006).
33. D. L. Moehring et al., Nature **449**, 68 (2007).
34. S. Olmschenk et al., Science **323**, 486 (2009).
35. W. Rosenfeld et al., Phys. Rev. Lett. **98**, 050504 (2007).
36. S.L. Braunstein and A. Mann, Phys. Rev. A **51**, R1727 (1995).
37. D.A. Lidar, I.L. Chuang, K.B. Whaley, Phys. Rev. Lett. **81**, 2594 (1998).
38. M.A. Nielsen and I.L. Chuang, *Quantum Computation and Quantum Information* (Cambridge University Press, Cambridge, 2000).
39. M. Razavi, M. Piani, and N. Lütkenhaus, arXiv:0810.5334.
40. O.A. Collins, S.D. Jenkins, A. Kuzmich, and T.A.B. Kennedy, Phys. Rev. Lett. **98**, 060502 (2007).
41. D.V. Vasilyev, I.V. Sokolov, E.S. Polzik, Phys. Rev. A **77**, 020302 (2008).
42. R.M. Macfarlane, J. Lumin. **100**, 1 (2002).
43. R.M. Macfarlane and R.M. Shelby, *Coherent Transients And Holeburning Spectroscopy In Rare Earth Ions In Solids; Spectroscopy Of Crystals Containing Rare Earth Ions* (Elsevier Science Publishers, Amsterdam, Netherlands, 1987).
44. E. Fraval, M.J. Sellars, and J.J. Longdell, Phys. Rev. Lett. **92**, 077601 (2004).
45. E. Fraval, M.J. Sellars, and J.J. Longdell, Phys. Rev. Lett. **95**, 030506 (2005).
46. J.J. Longdell, E. Fraval, M.J. Sellars, and N.B. Manson, Phys. Rev. Lett. **95**, 063601 (2005).
47. R. M. Macfarlane, J. Lumin. (1990)
48. J. Ruggiero, J.-L. Le Gouet, C. Simon, and T. Chaneliere, Phys. Rev. A **79**, 053851 (2009).
49. P.M. Ledingham *et al.*, arXiv:0906.4388.
50. S.A. Moiseev and S. Kröll, Phys. Rev. Lett. **87**, 173601 (2001).
51. M. Nilsson and S. Kröll, Opt. Comm. **247**, 393 (2005).
52. B. Kraus *et al.*, Phys. Rev. A **73**, 020302 (2006).
53. A.L. Alexander, J.J. Longdell, M.J. Sellars, and N.B. Manson, Phys. Rev. Lett. **96**, 043602 (2006).
54. N. Sangouard, C. Simon, M. Afzelius, and N. Gisin, Phys. Rev. A **75**, 032327 (2007).
55. A.L. Alexander, J.J. Longdell, M.J. Sellars, and N.B. Manson, J. Lumin. **127**, 94 (2007).
56. G. Hétet *et al.*, Phys. Rev. Lett. **100**, 023601 (2008).
57. J.J. Longdell, G. Hétet, P.K. Lam, and M.J. Sellars, Phys. Rev. A **78**, 032337 (2008).
58. B. Lauritzen *et al.*, Phys. Rev. Lett. **104**, 080502 (2010).
59. M. Afzelius, C. Simon, H. de Riedmatten, and N. Gisin, Phys. Rev. A **79**, 052329 (2009).
60. H. de Riedmatten, M. Afzelius, M.U. Staudt, C. Simon, and N. Gisin, Nature **456**, 773 (2008).
61. T. Chanelière, J. Ruggiero, M. Bonarota, M. Afzelius, and J.-L. Le Gouët, New J. Phys. **12**, 023025 (2010).
62. A. Amari *et al.*, arXiv:0911.2145.
63. M. Afzelius *et al.*, Phys. Rev. Lett. 104, 040503 (2010)
64. S.A. Moiseev and M.I. Noskov, Laser Phys. Lett. **1**, 303 (2004).
65. J. Nunn *et al.*, Phys. Rev. Lett. **101**, 260502 (2008).
66. F. Könz *et al.*, Phys. Rev. B **68**, 085109 (2003).
67. T. Böttger, C.W. Thiel, Y. Sun, and R.L. Cone, Phys. Rev. B **73**, 075101 (2006).
68. T. Böttger, C.W. Thiel, R.L. Cone, and Y. Sun, Phys. Rev. B **79**, 115104 (2009).

69. G.J. Pryde, M.J. Sellars, and N.B. Manson, Phys. Rev. Lett. **84**, 1152 (2000).

70. M. Nilsson *et al.*, Phys. Rev. B **70**, 214116 (2004).

71. L. Rippe *et al.*, Phys. Rev. A **71**, 062328 (2005).

72. B. Lauritzen *et al.*, Phys. Rev. A **78**, 043402 (2008).

73. S.A. Moiseev and W. Tittel, arXiv:0812.1730.

74. G. Hétet *et al.*, Opt. Lett. **33**, 2323 (2008).

75. J.-L. Le Gouët and P. Berman, Phys. Rev. A **80**, 012320 (2009).

76. M. Hosseini *et al.*, Nature **461**, 241 (2009).

77. M.U. Staudt *et al.*, Phys. Rev. Lett. **98**, 113601 (2007).

78. M.U. Staudt *et al.*, Phys. Rev. Lett. **99**, 173602 (2007).

79. M. Bonarota, J. Ruggiero, J.-L. Le Gouët, and T. Chanelière, arXiv:0911.4359.

80. M. Sabooni *et al.*, arXiv:0912.2525.

81. I. Usmani, M. Afzelius, H. de Riedmatten, and N. Gisin, arXiv:1002.3782, to appear in Nat. Comm.

82. A.L. Alexander, J.J. Longdell, and M.J. Sellars, J. Opt. Soc. Am. B **24**, 2479 (2007).

83. Y.S. Park *et al.*, Nano Lett. **6**, 2075 (2006).

84. C. Santori *et al.*, Phys. Rev. Lett. **97**, 247401 (2006).

85. A. Batalov *et al.*, Phys. Rev. Lett. **100**, 077401 (2008).

86. R. Kolesov *et al.*, Nat. Phys. **5**, 470 (2009).

87. F. Jelezko *et al.*, Phys. Rev. Lett. **92**, 076401 (2004).

88. P. Cappellaro, L. Jiang, J.S. Hodges, and M. D. Lukin, Phys. Rev. Lett. **102**, 210502 (2009).

89. N. Mizuochi *et al.*, Phys. Rev. B **80**, 041201(R) (2009).

90. M.V.G. Dutt *et al.*, Science **316**, 1312 (2007).

91. P. Tamarat *et al.*, Phys. Rev. Lett. **97**, 083002 (2006).

92. R. Alléaume *et al.*, New J. Phys. **6**, 92 (2004).

93. T. Gaebel *et al.*, New J. Phys. **6**, 98 (2004).

94. A. J. Shields, Nat. Photonics **1**, 215 (2007).

95. R. J. Young, S. J. Dewhurst, R. M. Stevenson, P. Atkinson, A. J. Bennett, M. B. Ward, K. Cooper, D. A. Ritchie, and A. J. Shields, New J. Phys. **9**, 365 (2007).

96. M. Kroutvar, Y. Ducommun, D. Heiss, M. Bichler, D. Schuh, G. Abstreiter, and J. J. Finley, Nature **432**, 81 (2004).

97. R. M. Stevenson, A. J. Hudson, A. J. Bennett, R. J. Young, C. A. Nicoll, D. A. Ritchie, and A. J. Shields, Phys. Rev. Lett. **101**, 170501 (2008).

98. O. Krebs, B. Eble, A. Lemaitre, P. Voisin, B. Urbaszek, T. Amand, and X. Marie, C. R. Phys. **9**, 874 (2008).

99. R. Hanson, L. P. Kouwenhoven, J. R. Petta, S. Tarucha, and L. M. K. Vandersypen, Rev. Mod. Phys. **79**, 1217 (2007).

100. A. V. Khaetskii, D. Loss, and L. Glazman, Phys. Rev. Lett. **88**, 186802 (2002).

101. W. A. Coish, V. N. Golovach, J. C. Egues, and D. Loss, Phys. Stat. Sol. (b) **243**, 3658 (2006).

102. I. A. Akimov, D. H. Feng, and F. Henneberger, Phys. Rev. Lett. **97**, 056602 (2006).

103. J. P. Reithmaier, G. Sek, A. Loffler, C. Hofmann, S. Kuhn, S. Reitzenstein, L. V. Keldysh, V. D. Kulakovskii, T. L. Reinecke, and A. Forchel, Nature **432**, 197 (2004).

104. K. Hennessy, A. Badolato, M. Winger, D. Gerace, M. Atatüre, S. Gulde, S. Fält, E. L. Hu and A. Imamoglu, Nature **445**, 896 (2007).

105. E. Peter, P. Senellart, D. Martrou, A. Lemaitre, J. Hours, J. M. Gerard, and J. Bloch, Phys. Rev. Lett. **95**, 067401 (2005).

106. D. Press, S. Götzinger, S. Reitzenstein, C. Hofmann, A. Löffler, M. Kamp, A. Forchel, and Y. Yamamoto, Phys. Rev. Lett. **98**, 117402 (2007).

107. C.Y. Hu *et al.*, Phys. Rev. B **78**, 085307 (2008); *ibid.* **78**, 125318 (2008); *ibid.* **80**, 205326 (2009).

108. A. J. Bennett, D. C. Unitt, P. See, A. J. Shields, P. Atkinson, K. Cooper, and D. A. Ritchie, Phys. Rev. B **72**, 033316 (2005).

109. M. B. Ward, O. Z. Karimov, D. C. Unitt, Z. L. Yuan, P. See, D. G. Gevaux, A. J. Shields, P. Atkinson and D. A. Ritchie, Appl. Phys. Lett. **86**, 201111 (2005).

110. M. Zukowski et al., Phys. Rev. Lett. **71**, 4287 (1993).

111. M. Weber et al., Phys. Rev. A **73**, 043406 (2006).

112. P. Maunz et al., Phys. Rev. Lett. **102**, 250502 (2009). (2007).

113. T. Wilk et al., Science **317**, 488 (2007); B. Weber at al., Phys. Rev. Lett. **102**, 030501 (2009).

114. W. Rosenfeld et al., Phys. Rev. Lett. **101**, 260403 (2008).

115. W. Rosenfeld et al., Adv. Sci. Lett. **2**, 469 (2009).

116. F. Henkel et al., *Highly efficient sub-μs photoionization detection of single* ^{87}Rb *atoms*, to be submitted to Phys. Rev. Lett., (2009).

117. D. N. Matsukevich et al., Phys. Rev. Lett. **100**, 150404 (2008).

118. M. Almendros et al., Phys. Rev. Lett. **103**, 213601 (2009).

119. M. K. Tey et al., Nature Physics **4**, 924-927 (2008).

120. R. Maiwald et al., Nature Physics **5**, 551 - 554 (2009).

121. K. Hammerer, E.S. Polzik, and J.I. Cirac, Phys. Rev. A **74**, 064301 (2006).

122. A.J. Hilliard *et al.*, Phys. Rev. A **78**, 051403 (2008).

123. B. Julsgaard, A. Kozhekin, and E.S. Polzik, Nature **413**, 400 (2001).

124. A.E. Kozhekin, K. Mølmer, and E. Polzik, Phys. Rev. A **62**, 033809 (2000).

125. I. Novikova *et al.*, Phys. Rev. Lett. **98**, 243602 (2007).

126. D. Oblak *et al.*, Eur. Phys. J. D **50**, 67 (2008).

127. J.F. Sherson *et al.*, Nature **443**, 557 (2006).

128. P.J. Windpassinger *et al.*, Phys. Rev. Lett. **100**, 103601 (2008).

129. J. Laurat *et al.*, New Journal of Physics **9**, 207 (2007).

130. D. N. Matsukevich *et al.*, Physical Review Letters **95**, 040405 (2005).

131. J. Nunn *et al*, Phys. Rev. A **75**, 011401 (2007).

132. A. V. Gorshkov *et al.*, Phys. Rev. Lett. **98**, 123601 (2007).

133. O. Mishina *et al.*, arXiv:0805.3353v1.

134. K.F. Reim *et al.*, arXiv:0912.2970.

135. K. Surmacz *et al.*, Phys. Rev. A **78**, 033806 (2008).

136. K. Surmacz *et al.*, Phys. Rev. A **74**, 050302 (2006).

137. R. Camacho, P. Vudyasetu, and J. Howell, Nature Photonics **3**, 103 (2009).

138. U. Schnorrberger *et al.*, Phys. Rev. Lett. **103**, 033003 (2009).

139. N. Bloembergen, Encounters in Nonlinear Optics: Selected Papers of Nicolaas Bloembergen, with Commentary , 375 (1996).

140. J. Nunn *et al.*, Phys. Rev. Lett. **101**, 260502 (2008).

141. K. Tordrup, A. Negretti, and K. Mølmer, Phys. Rev. Lett. **101**, 040501 (2008).

142. D. V. Vasilyev, I. V. Sokolov, and E. S. Polzik, Phys. Rev. A **77**, 020302 (2008).

143. D. N. Matsukevich and A. Kuzmich, Science **306**, 663 (2004).

144. T. Chaneliere *et al.*, Phys. Rev. Lett. **98**, 113602 (2007).

145. N. Sangouard *et al.*, arXiv:0912.3871.

146. E. Waks and C. Monroe, Phys. Rev. A **80**, 062330 (2009).

Approach	Potential Applications	Efficiency	Measurement	Fidelity	Entanglement with light	Band width	Storage Time	MM capacity	Dim.
RE AFC	SPS, QRep LOC4	0.34 / ~1	retrieval	0.97 cond.	not yet / Yes with PDC	100MHz / 1GHz	15μs / 30s	64 / high	high
NV	QRep, SPS	not yet / ~1 with cavity	direct	0.85	done	not yet / 10MHz	>100 μs / >10 ms	moderate	moderate
QD	SPS, QRep	~0.04 / ~1	retrieval	0.94	done	>GHz	2ns / 100 μs	high	low
Single atoms Free space	LHF, QRep	low / ~1 with cavity	direct	0.94 cond.	done	6MHz	150μs / >ms	moderate	moderate
Room-temp. gas	LOC4, Prec.msmt.	1	direct	0.7 uncond.	done	kHz / 100kHz	4ms / 200ms	low	high
Cold gas	Prec.msmt., LOC4, QRep	1	direct	0.75 uncond.	not yet / yes	1MHz / 0.5GHz	not yet / 100ms	moderate (spatial)	high
Raman gas	SPS, QRep	0.15 / ~1	retrieval	0.85 cond.	not yet / yes	1GHz / GHz	2μs / >100μs	moderate	high

Fig. 12. Overview of different approaches to quantum memories represented in the Integrated Projet *Qubit Applications*. The numbers shown are the best values that have been achieved by members of the project. **Approach:** RE AFC - Atomic Frequency Comb with Rare-Earth Doped Crystals (Geneva/Lund); NV - NV centers in diamond (Stuttgart); QD - Quantum Dots (Toshiba); Single atoms in free space (Munich); Room-temperature gas (Copenhagen); Cold gas (Copenhagen); Raman gas - Raman memory in a hot Cesium gas (Oxford). **Potential Applications:** See section 2 for a discussion of potential applications. SPS - Single-Photon Source; QRep - Quantum Repeaters; LOC4 - Protocols that allow a reduction in Communication Complexity using Memories and Local Operations and Classical Communication; LHF - Loophole-Free Bell experiment; Prec.msmt. - Precision measurement. **Efficiency:** See sections 4.2 and 6 for the concept of efficiency. Above the diagonal is the current experimental value, below the diagonal the value that appears in principle achievable with the respective approach. The same applies to the following columns. **Measurement:** In some approaches it is possible to measure the stored state in a way that is different from retrieving the stored light. In other approaches state measurements are done via retrieval. **Fidelity:** See sections 4.1 and 6 for the definition of fidelity. The given fidelities are conditional on detection of a photon, or unconditional as indicated. **Entanglement with Light:** Entanglement between an excitation stored in the memory and light has already been demonstrated in some approaches. **Bandwidth:** Bandwidth of the light that can be stored and retrieved (or that is emitted, cf. section 3.3). **Storage Time:** Maximal memory storage time. **MM capacity:** Capacity to store signals in multiple modes. **Dim.:** Capacity to store signals that live in a high-dimensional Hilbert space (for a single mode).